Analysis of Low Level Wind Shear Flight Perturbations on Final Approach Using QAR Data

A Particular Case of Madeira Airport

Sérgio Vasco Guerra de Sousa Silva

Thesis to obtain the Master of Science Degree in

Aerospace Engineering

Supervisor: Prof. Afzal Suleman

Examination Committee

Chairperson:	Prof. Fernando José Parracho Lau
Supervisor:	Prof. Afzal Suleman
Members of the Committee:	Prof. Pedro da Graça Tavares Alvares Serrão

October 2022

Declaração:

Declaro que o presente documento é um trabalho original da minha autoria e que cumpre todos os requisitos do Código de Conduta e Boas Práticas da Universidade de Lisboa.

Declaration

I declare that this document is an original work of my own authorship and that it fulfills all the requirements of the Code of Conduct and Good Practices of the Universidade de Lisboa.

Sérgio S. Silva

Acknowledgements

I would like to thank:

Prof. Afzal Suleman for his unrelenting support during the extensive time in which this thesis was under works as well as the wise counseling.

TAP Air Portugal Safety team: Gonçalo Nápoles, Emílio Pereira, Rui Alves, Yannick Duarte, Pedro Santos, João Silva for their support and guidance on QAR data exploitation.

Dr. Víctor Prior (IPMA), for his wise advice on specific Madeira conditions and counseling on weather data acquisition and interpretation.

Eng. Vítor Pelado, from APPLA, for the framing of his previous work on operational conditions at Madeira Airport.

Eng. Rute Ramalho (ANAC), for the historical framing and facilitation of available data.

My parents, for the principles that they taught me on my early life.

Finally and most importantly, my dear wife, Beatriz for the continued support and encouragement and my sons Miguel and Tiago for their comprehension for all the time that I was not available to be with them.

Thank you!

Abstract

The final stages of approach to landing are a critical part of the flight of an aircraft. This phase of flight is characterized by low speed and proximity to the ground, with minimal levels of energy, thus rendering the aircraft vulnerable to atmospheric perturbations and in greater danger of uncontrolled ground contact. The low level wind shear and turbulence are quasi-stochastic phenomena that introduce difficulties on the flight path control of landing aircraft and must be dully considered on the interest of safety.

Due to local weather patterns and terrain configuration, one particular case were these atmospheric phenomena play an important role and impose operational limitations is the Madeira International Airport.

This work fuses aircraft data from Quick Access Recorders with surface wind at Madeira Airport and analyzes some key aircraft parameters and reactions in correlation to surface wind observed.

Data cleaning, filtering and smoothing is described, particularly by the use of a Rauch-Tung-Striebel algorithm, as well as side slip angle estimation and calibration of data from angle-of-attack sensors for overall data coherence.

Spot wind vector components are extracted from QAR data, and various turbulence and flight hazard metrics are analyzed in light of the wind conditions, including the achievement of stabilization criteria, standard practice in air transport industry.

Given a specific wind direction at the touchdown point, no definitive geospatial correlation is found between flight perturbations and wind conditions except the increase of stochastic turbulence connected with higher surface wind intensities.

Keywords

Windshear, QAR, Rauch-Tung-Striebel, Turbulence, Madeira Airport

Resumo

A fase final de aproximação para aterragem é uma parte crítica do voo de uma aeronave. Esta fase é caracterizada por baixas velocidades e proximidade à superfície, com níveis de energia mínimos, deixando assim a aeronave mais vulnerável a perturbações atmosféricas e em maior perigo de contacto não controlado com o chão. O cisalhamento de vento de baixa altitude e a turbulência são fenómenos quase-estocásticos que introduzem dificuldades no controlo do voo perto da aterragem e devem ser devidamente considerados em prol da segurança.

Devido aos padrões meteorológicos locais e configuração do terreno, um caso particular em que os fenómenos atmosféricos desempenham um papel particularmente importante é no Aeroporto Internacional da Madeira.

Este trabalho faz a fusão de dados recolhidos nos gravadores de voo de aeronaves com os ventos registados à superfície no aeroporto da Madeira e analisa alguns dos parâmetros fundamentais da aeronave e das suas reações, procurando estabelecer uma correlação destas com o vento observado.

A limpeza, filtragem e amaciamento dos dados é descrita, com particular ênfase para o uso do algoritmo conhecido como Rauch-Tung-Striebel, bem assim como a estima do ângulo de derrapagem e calibração dos dados de ângulo-de-ataque para coerência global dos dados.

São também estimadas, a partir dos dados do Gravador de Voo, as componentes do vento local e com base nestas são analisadas algumas métricas de perigo para o voo, incluindo o cumprimento dos critérios de estabilização comuns na indústria de transporte aéreo.

Tendo em conta uma direção de vento à superfície fixa, escolhida, não foi encontrada uma correlação geoespacial entre as perturbações no voo e as condições de vento à superfície, exceto o aumento do efeito estocástico da turbulência relacionado com intensidades mais fortes.

Palavras Chave

Cisalhamento de Vento, QAR, Rauch-Tung-Striebel, Turbulência, Aeroporto da Madeira

Table of Contents

List of Figures

List of Tables

Abbreviations

AAL – Above Airdrome Level

AGL – Above Ground Level

AGS – Analysis Ground Station

AIDS – Aircraft Integrated Data System

AMSL – Above Mean Sea Level

AOA – Angle of Attack

CVR – Cockpit Voice Recorder

DAR – Digital AIDS Recorder

DFDF – Digital Flight Data Recorder

EASA – European Aeronautical Safety Agency

EDR – Eddy Dissipation Rate

FAA – Federal Aviation Administration

FCOM – Flight Crew Operating Manual

FDM – Flight Data Monitoring

FDR – Flight Data Recorder

FOQA – Flight Operations Quality Assurance

ft – feet (0.3048 m)

GNSS – Global Navigation Satellite System

IFR – Instrument Flight Rules

ILS – Instrument Landing System

LIDAR – Light Detection and Ranging

MOQA – Maintenance Operations Quality Assurance

MTOM – Maximum Take-Off Mass

Nm – Nautical Mile (1852 m)

PAPI – Precision Approach Path Indicator

QAR – Quick Access Recorder

RNP (AR) – Required Navigation Performance (Authorization Required)

TSO – Technical Specification Order

VFR – Visual Flight Rules

VOR – Very High Frequency Omnidirectional Range

WMO – World Meteorological Organization

Nomenclature

x, y, z	Positions	Subscripts	
X, Y, Z	Forces along x, y, z	e	Inertial reference
u, v, w	Velocities along x, y, z	b	Body reference
p, q, r	Angular rates around x, y, z	a	Air Mass reference
C_L, C_D	Coefficient of Lift, … Drag	w	Wind
θ, ϕ, ψ	Angles of pitch, roll and heading		
α, β	Angle of attack, …sideslip		
γ, χ	Flight path angle, Track angle		
φ, λ	Latitude, Longitude		
A	Aspect ratio		
b	Wing Span		
S	Area		
$c, \bar{c}$	Chord, Mean chord		
Λ	Sweep angle		
C_{l_α}, C_{L_α}	Gradient of C_L with α: 2d airfoil, 3d wing		
Q	Dynamic pressure ($\frac{1}{2}\rho V^2$)		
R	Radius of curvature along the meridian ellipse		
N	Radius of curvature along the first vertical		

1 Introduction

1.1 Motivation

The final stages of approach to landing are a critical part of the flight of an aircraft. This phase of flight is characterized by low speed and proximity to the ground, with minimal levels of energy, thus rendering the aircraft vulnerable to atmospheric perturbations and in greater danger of uncontrolled ground contact. In fact, 54% of fatal accidents on commercial aviation in the period of 2011 – 2020 have occurred in the Final Approach and Landing[1], highlighting the sensitivity of this flight phase.

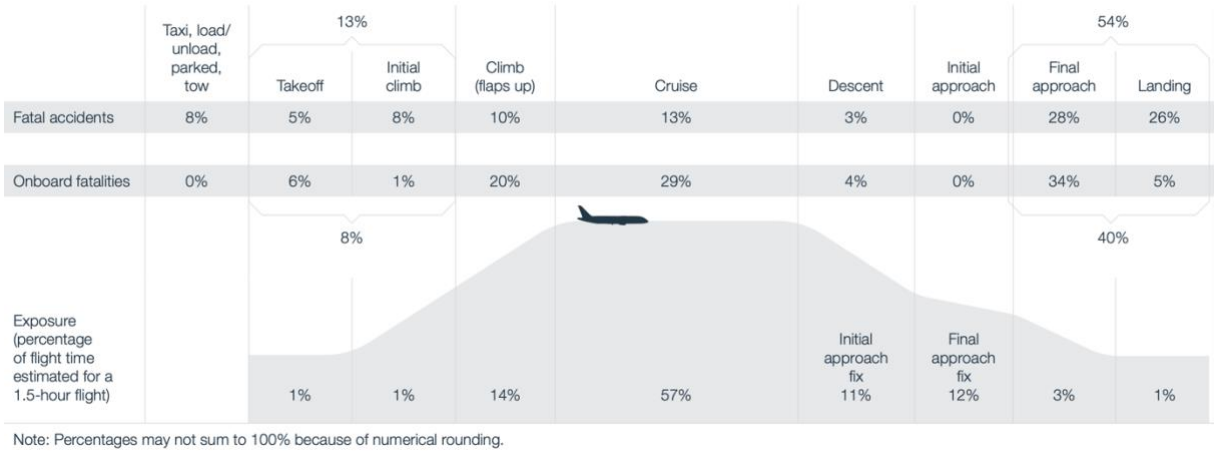

Figure 1.1 - Fatal accidents and fatalities per phase of flight. [1]

Two cases of significant perturbations that can be accounted for are the low-level turbulence and the low-level wind shear. Both introduce challenges on the control of the flight and on the maintenance of adequate speed, flight path and general aircraft control.

A distinction is made here between these phenomena as the first is understood as a stochastic process whereby considering a sufficient distance, the vectorial sum of all movements of air mass tend to cancel out, while the latter results in a permanent and relatively sudden, shift in direction and or velocity of the wind.

Although there are several equipment today that can scan the approach path and advise pilots of significant turbulence or wind shear (most notably the LIDAR), these systems have a cost such that very few airports consider their implementation. Usually, the pilots of landing aircraft estimate the turbulence on final approach either through reports of previous aircraft or based on their observation, experience and surface wind information given by Air Traffic Control.

Some airports, due to their environment have conditions that are more prone to develop low-level turbulence or wind shear. Such conditions include the presence of significant obstacles upwind of the approach path, such as large buildings, hills or lines of tall trees. Depending on the configuration, the

presence of hills may cause downdrafts or localized wind acceleration due to funneling on valleys or venturi-like effects [2].

One case where these phenomena compound together and cause restrictions in operations is at the Madeira International Airport. The conjunction of runway location, orographic features and the prevailing wind direction makes this airport notorious for its challenging approaches even on moderate winds.

In order to mitigate the operational risk at this airport, a set of measures have been implemented which include special requirements of pilot training, a minimum experience on the aircraft type and an enforcement of sectorial wind limits above which the operation is forbidden[3]. These wind limits have been established in the 1970's and, albeit some minor revisions, are still in force today since there is no solid evidence that these could be relaxed while keeping the desired level of safety.

In the year 2019 (taken as reference because is pre-pandemic) Madeira International Airport had nearly 12 000 landings serving a total of 3.2 million passengers [4]. A statistical appraisal of the first 100 days of 2018 revealed that on this period around 550 movements and 80 000 passengers have been affected by flight delays or cancellations due to wind conditions, with the corresponding economic impact for the passengers themselves, the airlines and the region, which is heavily dependent on tourism[5].

This economic and operational loss has prompted the authorities and stakeholders throughout the years to promote a number of studies regarding the wind flow around the airport in order to judge the validity of the sectorial wind limits and eventually propose that these could possibly be better tailored to modern aircraft and operational reality. Thus far, to the knowledge of the author, none has included the use aircraft flight recorder data to measure quantitatively the flight perturbations introduced on the approach phase.

Indeed, all turbine powered aircraft with a Maximum Take-off Mass (MTOM) above 5 700kg certified after 2004 are required by regulations to carry on board a Flight Data Recorder (FDR) that records a set of at least 78 key parameters [6] which are usually available for download and analysis after flight. This data is routinely exploited by the airlines under Flight Data Monitoring (FDM) programs whose main objective is to monitor the safety of operations. It is expected on this thesis that through the analysis of these parameters the principal flight perturbations on final approach to Madeira Airport are quantified so that a greater insight is achieved on the influence that certain wind regimes have on aircraft.

1.2 Objectives

The main objective of this thesis is to investigate the existence of a correlation between the flight perturbations as measured by the Flight Data Recorders with the surface wind conditions observed at the airport.

To achieve this goal a preparatory work must be done involving the processing and analysis of a significant amount of data. Two primary datasets were compiled as the source of information for the study: One of the wind direction and intensity at four different locations in the airport and other of selected parameters of the FDR records of landing aircraft. By the focus of this study, which is more

leaned towards heavier wind conditions and turbulence, one can appreciate that the two datasets present their own challenges for real usefulness. The wind, by its nature reveals a quasi-stochastic behavior with constant variations in direction and intensity whereas the QAR records have a significant number of parameters which require calibration, smoothing and filtering. So, the careful selection and cleaning of data is of paramount importance for the quality of the results.

A second objective is to extract from the QAR data a tri-dimensional wind vector as felt by the aircraft in flight. It was found during the preliminary works that both the aircraft systems and the Analysis Ground Station (AGS) that are used to process the QAR data only provide horizontal components of the wind. The Data Analysts working on Flight Safety FOQA programs regard that information as important and, at current day, if such information is sought, the processing of data must be outsourced.

Finally, it is also an objective to exploit the data and through the application of some existing hazard metrics analyze the prevailing perturbations on the aircraft and compare with commonly accepted margins for safe operation.

1.3 Scope

This study is centered on the medium class of commercial air transport aircraft of the type Airbus A320 and the data used pertains to A319, A320 and A321 models operated by TAP Air Portugal. These are single-aisle medium range aircraft, with fly-by-wire flight controls and landing masses ranging from around 55 000 kg up to 77 800 kg. Coincidently, this is the most common type of aircraft at Madeira International Airport representing over 50% of all movements [7].

The flight phase analyzed is the approach segment from 300' AAL (Above Airdrome Level) until touchdown, as it is the portion where flight perturbations represent the most hazard.

It is plausible that the type and strength of low-level windshear and turbulence is dependent on geographic location, altitude, wind direction and intensity - hence the sectorial operational limitations. In order to contain the greatest number of variables, only the approaches to runway 05 and wind from direction of 350º (± 5º) magnetic will be considered.

The main interest in this work is to establish a data processing methodology and establish a proof of concept. The approaches to runway 23 and all other various wind directions could be separately analyzed in the same method, if that would be of interest.

1.4 Previous Work and State of the Art

The exploitation of FDR data is not at all new - indeed is as old as the FDRs themselves. Nevertheless, a number of challenges resides on the quality of the data as it is affected by problems of sensor bias, inaccuracy, low sample rates and desynchronization. Haverdings and Chan[8] give an approach to the data processing using a Kalman filter-smoother, calibration of sensors by multiple regression analysis and clues to parameter extraction. Höhndorf *et al*[9] worked on techniques for the reconstruction of aircraft states during approach and landing by using a Rauch-Tung-Striebel filter-

smoother and proposed some sensible values for the covariance matrices to be used. Additionally, a method of parameter estimation is employed by Sembiring et al[10] which allows for a correction of bias/systemic errors and better accuracy of parameters as well as a method for extracting wind components on Earth frame. Also, Huang et al[11] provide a method for vertical wind component extraction from the available QAR data as well as AOA calibration.

On the effects of wind shear on approach there is significant body of work, mostly condensed already by ICAO on its Doc 9817[2] where all the major aspects of Low Level Wind shear are treated. The determination of wind shear intensity criteria which aims at establishing a way to quantify the hazard of this phenomenon, is presented both on the version proposed by Woodfield and Woods and also on the one proposed by Swolinsky. Also the EASA and FAA criteria for Airborne wind shear warning and escape guidance systems for transport airplanes is presented, as determined on TSO-C117a[12]. This criteria is based on a factor (denominated F-factor) which was first proposed by Bowles[13] and reflects the aircraft's rate of change of the energy state over a certain period of time.

As for the turbulence, the original work of Cornman et al [14] has been adopted by the World Meteorological Organization and ICAO [15] for the aeronautical evaluation and reporting of turbulence. The method is designated the Eddy Dissipation Rate (EDR) and attempts to describe the gust spectrum around the aircraft on a single parameter. For the practical implementation, a method of calculation is proposed by Haverdings and Chan [16] and also by Huang, Sun *et al*[11].

On the subject of acceptable flight perturbations during final approach, extensive work on metrics and criteria has been developed since 1970's by NASA Ames and Langley Research Centers in connection to the study of Wake Vortex Encounter or wind shear, but no definite industry or scientific consensus has been established[6],[7],[19],[20]. This is because, on one hand, the perception of hazard is inherently subjective, and on the other, very dependent on a large variety of conditions that are nearly impossible to conjugate on a practical manner. Sammonds and Stinnett [17] proposed a maximum bank angle and roll acceleration dependent on altitude which seem to have gathered a good data consistency and was further confirmed and improved by also considering the concept of RCR (Roll Control Ratio) on the European S-WAKE project in 2004 by Luckner *et al*[21]. On wind variations in horizontal plane, a study made at the NLR by Nieuwpoort *et al*[22] suggests that below 200' the mean wind variation should be kept under a certain threshold in order to maintain an adequate flight path control.

1.5 Thesis layout.

Firstly, an overview of the operational conditions and weather environment encountered at Madeira Airport are presented, including the wind data gathering infrastructure followed by a brief presentation of the aircraft types from where data was gathered and respective equipment (QAR).

Then, a description is made of the data filtering, smoothing, calibration and validation techniques used, most notably the use of the Rausch-Tung-Striebel method, of the family of the Kalman Filter methods.

A description is also made on the geospatial positioning adjustments for the overall coherence of the flight path, on the angle-of-attack sensor data calibration and on the method of estimation of side slip angle.

From this processed data the 3D wind components are estimated and, according to defined wind intensity categories, plotted as a function of distance to the runway. Based on these wind components and vertical accelerations felt on the aircraft, some turbulence metrics are analyzed as well as hazard metrics.

Finally, conclusions are drawn from the results and a set of future possible work expansions on this topic are suggested.

2 Background

2.1 Madeira International Airport

Madeira island is the largest of the archipelago of the same name, situated in the subtropical eastern North Atlantic with approximate coordinates of 32.7º N latitude and 17.0º W longitude. The island is comprised mostly of complex steeply rising terrain, being characterized by a mountainous formation of approximately 50 km by 20 km.

The airport is located on the southwest coast, at an altitude of 51 m (191') featuring a single runway of 2481 x 45 m, with the designation 05/23.

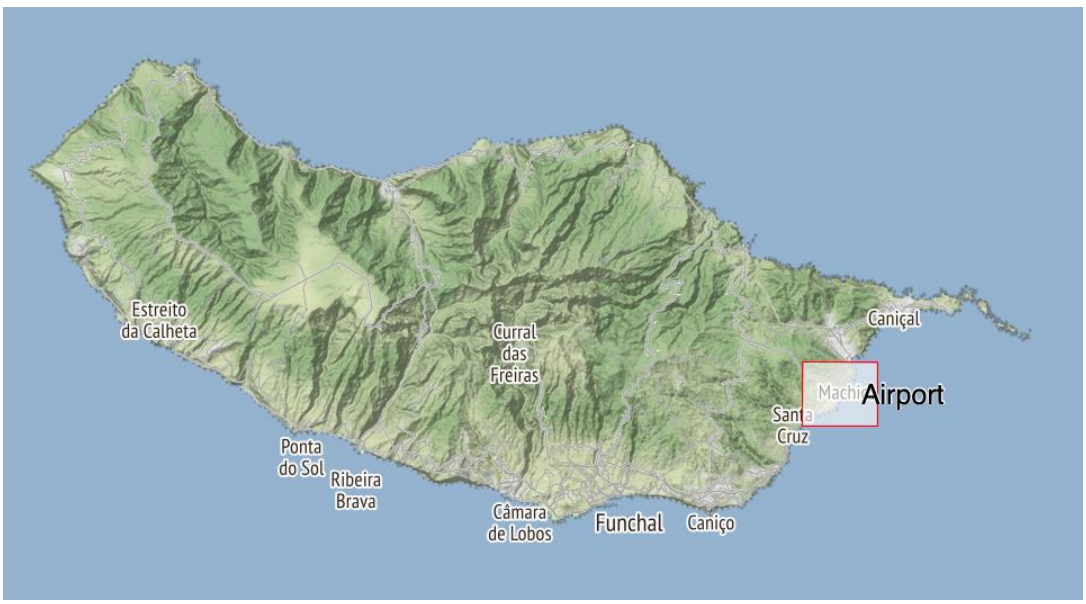

Figure 2.1 – General arrangement of Madeira island and airport location [source:SNIG.pt].

The runway environment is characterized by the upwards steep inclines to the NW and downwards on other directions (see Figure 2.2).

Due to terrain altimetry most approaches are completed through a *circling approach*, that is, a visual maneuver where the pilot brings the aircraft to a position from where a normal landing can be made on a runway that is otherwise not suitably located for a *straight-in approach*. Most notably, landing on runway 05 is accomplished by flying a curved path with final line-up at about 1 nm from threshold. On the vertical plane, a nominal 3º glide is indicated by PAPI system installed on both sides of runway.

2.2 Winds

2.2.1 Synoptic

The overall weather in Madeira is strongly influenced by the presence of a semi-permanent subtropical anticyclone over the North Atlantic. From Spring to Autumn, the predominant wind direction

is from north to northeast, which, due to the orientation and morphology of the island, fosters the conditions for a large-scale wake formation. The airport, due to its location, is often affected by the turbulence of this wake[23]

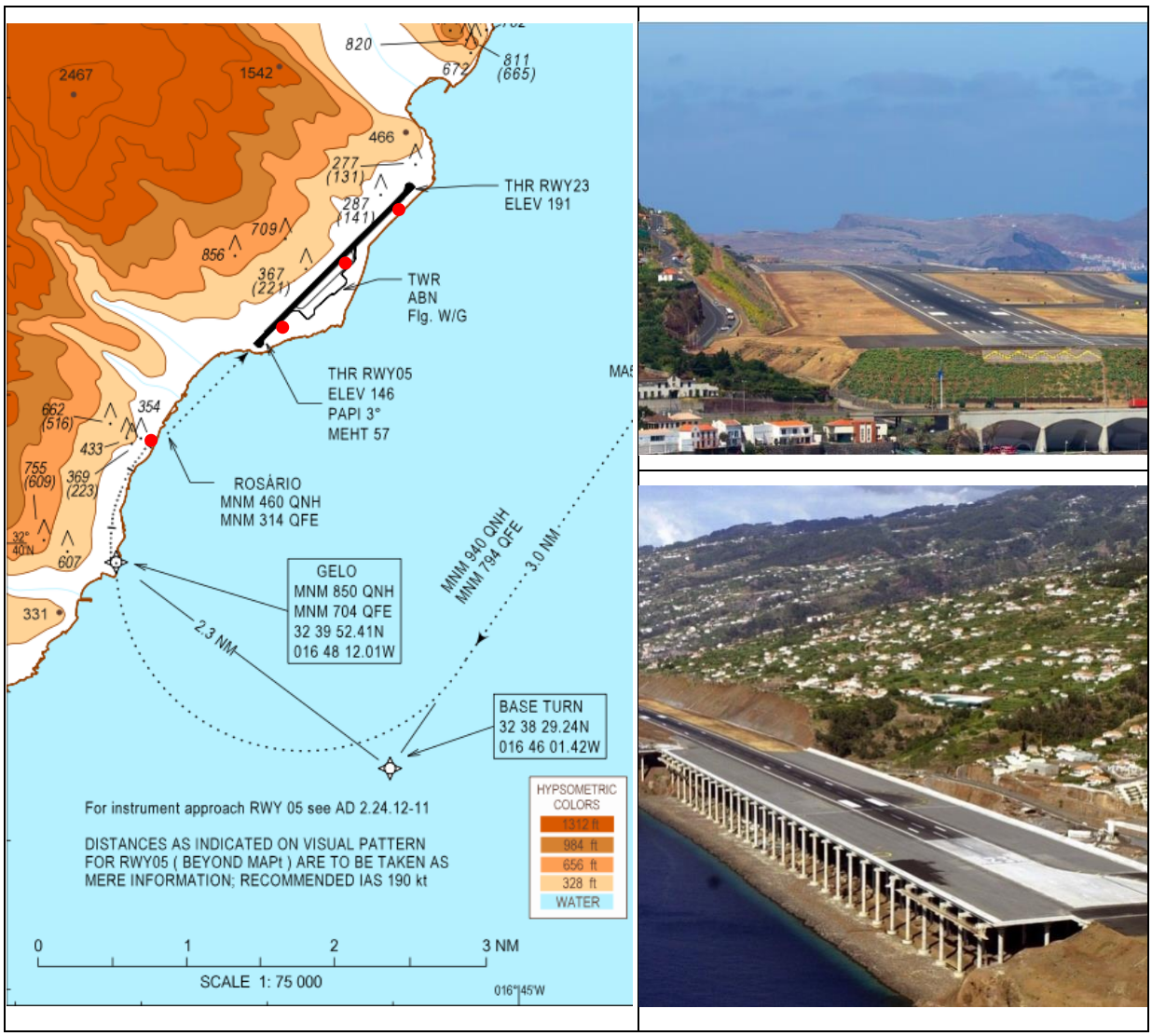

Figure 2.2 - Left: Airport framing with surrounding terrain showing the path of curved approach to runway 05 (dotted line) and position of anemometers (red dots)[3]; Top right: Threshold of runway 05 with visible sloping terrain to the left [24]; Bottom right: Threshold runway 23.[25]

2.2.2 Surface Wind Sensors and Wind Data

A network of four *Vaisala Windset WA15* comprised each of an anemometer and a wind vane are installed on the airport. They are located close to:

- touchdown point Rwy05
- touchdown point Rwy23
- mid runway
- Rosário, about 1 nm before the threshold of Rwy05

These sensors record at 10 second interval the instantaneous intensity and direction of wind. Additionally, for operational use, also a 2 minute and 10 minute average and maximum are computed and recorded.

Figure 2.3 - Vaisala Windset WA15. [vaisala.com]

2.2.3 Operational Limitations

The sectorial wind limitations have been established in the 1970's and although several studies led to minor changes and adaptations through the years, the essential magnitude of the limitations remain in force.

Also, in 1986 the runway was extended from the original 1600 m to 1800 m and in 2002 a major intervention extended the runway to the actual 2780 m while rotating its axis a few degrees, which raised the question of the need to re-evaluate the criteria.

There are different wind limitations for take-off and landing, the latter being more restrictive and most affecting the operation. The representation of the sectors may be observed on Figure 2.4, by magnetic bearings, and maximum intensities of wind for landing. These limits are generally referred to the touchdown point anemometer, with the direction and intensity being averaged over 2 minutes and the '*gust*' is the maximum intensity in the same 2 minutes. There are additional conditions for the sector 200º - 230º (marked with '*' on Figure 2.4) which are not relevant for this work.

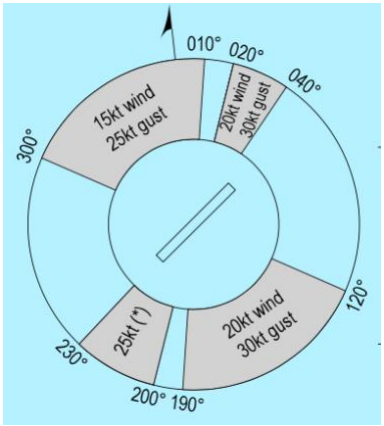

Figure 2.4 - Sectorial wind limitations for landing at Madeira in 2022 [3].

2.3 Approach Aids

There are several instrument approaches to the airport, either based on VOR or on GNSS. The most common of these are intended for guidance down through cloud breaking followed by visual approach. There are also higher precision GNSS approaches, designated RNP-AR (AR stands for “Authorization Required”) which takes the aircraft down to around 300’ AAL and 1 nm from the runway. These more precise approaches require a special authorization from the Aeronautical Authority as well as specific training by the crew and adequately equipped aircraft, as a navigation system with high accuracy is mandatory.

The final approach vertical guidance is accomplished through the use of PAPI, which in the case of runway 05 is installed on both sides of the runway and having the right set directed slightly outward from centerline. This system consists of four lights in a horizontal line which illuminate white or red depending on the vertical angle of observation. See Figure 2.5.

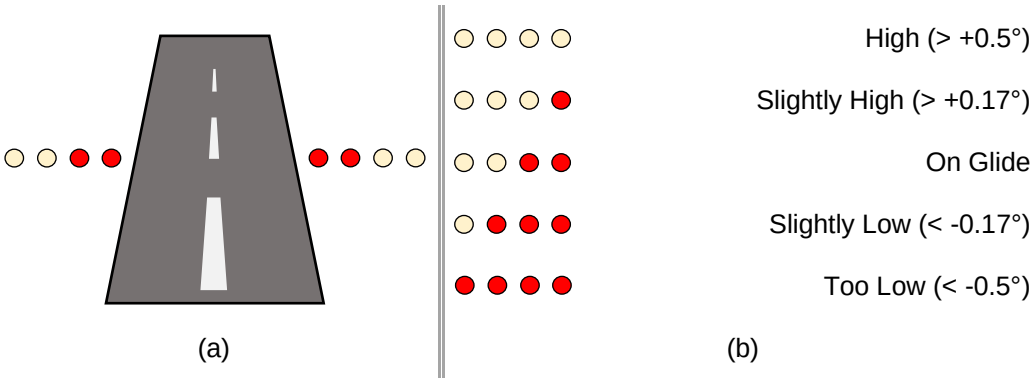

Figure 2.5 - PAPI (Precision Approach Landing System) description. (a) Location relative to runway; (b) Color encoding.

2.4 Operation

The approach to runway 05 is flown either visually as depicted on Figure 2.2 or via the use of an RNP-AR instrument approach. For the purpose of this work there is no significant difference. At the end of the downwind leg (Base Turn) the aircraft is set to the final configuration, with landing gear down and

flaps/slats in *CONF 3* or *CONF FULL*, at pilot option – These are the approved settings for landing as per Airbus FCOM. *CONF 3* corresponds to a lesser extension of lift devices and causes higher airspeed on approach, thus higher kinetic energy, with the corresponding effect on maneuverability and landing distance.

The checkpoint '*GELO'* should be crossed at a minimum of 850' AMSL (704' AAL) which sets the aircraft on approximately a conventional 3º glide angle, following the PAPI indications to touchdown. Final line-up with runway is achieved by point '*ROSÁRIO*' and the runway threshold is crossed at a height of 57'.

Landing clearance is given before the aircraft reaches certain points depending on the 2 minute average winds on touchdown anemometer being within limits, otherwise go-around instructions are provided.

The approach from Base Turn until landing is always flown manually (Auto Pilot OFF) except on the RNP-AR instrument approach, where Auto Pilot may be disconnected only at 380 ft AAL.

2.4.1 Applicability of the 'Stabilized Approach' concept

One of the air transport industry agreed safety standards is the stabilized approach concept. This amounts generically to the attainment and conservation of certain key parameters (airspeed, pitch, roll, thrust, configuration) in a defined range during the last stages of the approach – typically bellow 1000', with some parameters allowed to stabilize as low as 500' AAL, until touchdown. Regarding the risk of accident on the landing phase, it is well established by statistical evidence that over 60% of incidents and accidents on landing have an unstabilized approach as a causal factor [26]. Although these criteria are designed and specially well suited for the most common straight-in, ILS-like approach, it is still applicable to this special case of curved approach, albeit some adaptations, namely in what regards to lateral deviations, which must only be considered after point 'ROSÁRIO'.

These main stabilization criteria are, at and below 1000' AAL:

- Aircraft in final configuration for landing (Landing Gear and Flaps);
- On the glide path (as indicated by PAPI);
- On the extended Centerline of Runway (with the exception stated above);
- At target speed for the approach;
- Engine power stabilized at a setting usually above Idle.

An additional set of criteria is usually implemented by operators to give guidance on 'alert' triggers for certain key parameters. The purpose of these is that pilots call them out aloud if they are attained during the approach to raise the awareness of the crew and prompt for an immediate correction. As such, is operationally acceptable if some small, momentary and involuntary excursions occur, as long as these are recognized and promptly corrected.

Although these differ among operators and aircraft type, some examples of the envelope until the alert triggers are:

- Bank angle not more than 7º;
- Pitch angle between -2.5° and +7.5º;
- Descent rate of less than 1000 ft/min;
- Airspeed between target speed -5 kts and +10 kts;
- When on ILS, within 1 dot of the GS (±0.4º). When on visual, maintain correct GS indications on the Approach Path Indicator (in the case of PAPI, the correct glide path indication is obtained on roughly ±0.17º)

There criteria are further analyzed and discussed on section 4.3.3.

2.5 Aircraft

2.5.1 General

The aircraft used as source of data is the Airbus A320 family of subsonic medium-range civil transport in the following 3 models: A319, A320 and A321. These models differ mainly on fuselage length and maximum masses, being otherwise very similar. Also, there is a mix of different engine configurations as some of the data is prevenient from aircraft equipped with CFM56-5B (CEO) and others with LEAP1A (NEO) but this does not change the aerodynamic characteristic in any significant way.

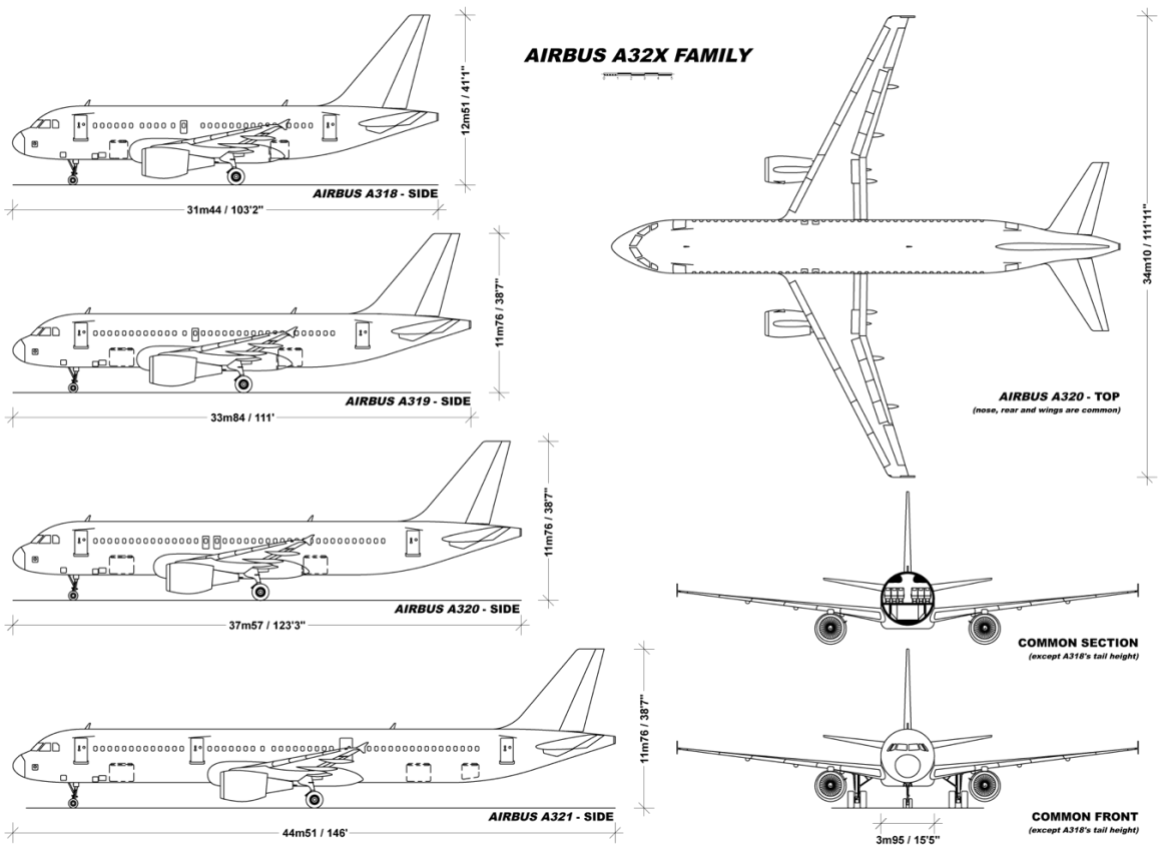

Figure 2.6 - Diagram of Airbus A32x family. [27]

These aircraft have fly-by-wire controls with several features of flight stabilization which present to the pilot a more benign set of flight characteristics when compared to conventionally controlled aircraft. This is because the flight control computers automatically deflect the control surfaces in response to perturbations striving to keep the key flight parameters at nominal values. Nevertheless, this is far from eliminating sudden perturbations such as those induced by turbulence or windshear.

2.5.2 Flight Data Recording

There are several recorders in the aircraft:

- DFDR – Digital Flight Data Recorder

  It is a crash proof recorder, mandatory by regulations [6], usually installed on the tail of the aircraft, aimed at forensic analysis and is able to store 25 hours of data comprising at least 82 parameters but it is normal practice that it records over 2000 parameters. This is popularly known as the '*black box*'.

- QAR – Quick Access Recorder

  Stores the same parameters as the DFDR but is installed on the avionics bay and the data can be easily extracted through a digital storage media or, on recent models, through a wireless datalink. This data is routinely used by the operators for their Flight Data Monitoring programs (FOQA and MOQA) which are aimed at identifying operational and maintenance opportunities for enhancing safety and efficiency of flight operations.

  This is the source of data for this work.

- DAR – Digital (Aircraft Integrated Data System) Recorder

  It is an optional, airline customizable recorder, using essentially the same protocols as the DFDR and QAR, but tailored to produce automatic specialized reports to be used by different company departments for management.

- CVR – Cockpit Voice Recorder

  It is a mandatory, crash proof recorder, usually installed at the tail of aircraft and may be combined with the DFDR. Its purpose it is to record not only cockpit sounds but also radio and cabin communications for forensic treatment.

Figure 2.7 - Left: Examples of DFDR and CVR; Right: Example of a wireless QAR [28]

The DFDR and QAR are connected to aircraft systems through a Flight Data Interface and Management Unit which collects and serializes the data for recording.

In this work, the term FDR (Flight Data Recorder) will be used as a general umbrella term for this type of device without regard to the specific designation of each component.

2.6 Flight Data Analysis Software (Ground Station)

A PC based software is capable of reading and decoding the flight recorder's data. The processing is customizable so that different analysis can be performed for the purposes of flight safety, maintenance, fleet management, etc.

The raw data, as decoded by this station, is the main source for this thesis.

3 Data Gathering and Preprocessing

3.1 Data Gathering

3.1.1 General considerations about the use of data from FDR

For reasons of data protection, all the flight data released for this study was de-identified; This means that no data can be connected to the specific flight that gave origin to it. To preserve this fundamental requirement and concurrently maintain the necessary correspondence with the weather records at the time of landing, a small program written in Python language was developed and delivered to TAP Air Portugal so that the Data Analysts could automatically insert the wind records in the flight data at the correct times and then remove all the date/time references as well as aircraft identification.

3.1.2 Meteorological Data

The data records for wind intensity and direction from the four anemometers (Rosário, threshold runway 05, mid runway and threshold runway 23) was obtained in *.csv* format for the years of 2018 and 2019. The records are timestamped, spaced at 10 seconds interval and are instantaneous values.

For this study only the direction of 350º±5º magnetic at the threshold of runway 05 was chosen for analysis because it is anecdoticaly known by pilots to cause challenges on aircraft control during approach and it is at the heart of the most restrictive sector.

Using a routine in Python programming language, periods of wind data that average the direction of interest were selected and extracted to provide intervals of time for candidate flight selection.

In terms of meteorological reporting, the wind that the ATC must report to aircraft before landing is a 2 minute average, with additional provisions for gust reporting and directional variation. For this reason, only flights that present the relevant average wind direction during the last 2 minutes before touchdown are analyzed.

3.1.3 Flight Selection

A list of all the flights operated by TAP Air Portugal that landed in Madeira Airport in 2018 and 2019 was compiled, with the date/time of landing, flight number and tail number of the aircraft involved, generating just over 7800 records. After crossing this database with the selected winds, a list of nearly 600 flights of interest was generated. These were extracted from the Ground Station database and de-identified (as described on 3.1.1) and of these, circa 540 were retrieved as usable data. At this stage, with accurate wind data already attached, only the flights that had the 2 minute before landing average direction in the sector of interest (350º±5º) were selected, amounting to 161 datasets.

3.2 Preprocessing

3.2.1 Raw data presentation

Raw data was delivered in *.csv* format, one file per flight, and presented some challenges that had to be dully addressed before further work could be done.

- Different parameters are presented at different sampling frequencies (see Table 1 and Annex 1) - from 4 Hz to 0,25 Hz;
- Records are not fully synchronized, that is, the data presented at a certain line may have been acquired somewhere in the time interval between previous record and the actual;
- Some parameters have a definition that is less than desirable for the type of analysis envisaged (e.g., pitch angle is presented in 0.35º increments, rounded to 0.1º);
- Some parameters have a sampling rate lower than desirable (e.g., AOA is sampled at only 1Hz)
- Most of the parameters have noise and bias (e.g., Position Latitude/Longitude, AOA)

Table 1 - Raw data of FDR as extracted from Ground Station.

TIME	GWC	LONFM_1	LATFM_1	BALT_1	RALT1	PITCH	PITCH_RATE	HEAD_MAG	PTCR	ROLR	YAW	LONG	LATG	IAS	TAS	AOAL	AOAR
0	61,92					3,2	-0,1		-0,1	-0,1	0	0,07	-0,01		233	3,3	3,9
0,25		-16,60118	32,89884	3095		3,2	-0,1	233	-0,1			0,07	0	225			
0,5					3106	3,2	-0,1		-0,1	0	0	0,07	0				
0,75						2,8	-0,1		-0,1			0,07	-0,01				
1	61,92					2,8	-0,1		-0,1	-0,5	-0,1	0,07	0		233	3,4	4
1,25		-16,60255	32,89746	3091		2,8	-0,1	233	-0,1			0,07	0	226			
1,5						2,8	-0,1		-0,1	0,1	-0,1	0,07	0,01				
1,75						2,8	-0,1		0			0,06	0				
2	61,92					2,8	-0,1		0	0,3	-0,2	0,06	0		233	3,3	3,8
2,25		-16,60324	32,89678	3086		2,8	0	233	0,2			0,07	0	226			
2,5					3103	3,2	0		0,5	-0,2	-0,2	0,07	0				
2,75						3,2	0,2		0,5			0,07	-0,01				
3	61,92					3,2	0,3		0,4	-0,1	-0,1	0,07	0		234	3,3	3,9
3,25		-16,60461	32,89609	3082		3,5	0,3	233	0,4			0,07	-0,01	227			
3,5						3,5	0,4		0,3	-0,2	-0,1	0,07	-0,01				
3,75						3,5	0,3		0,1			0,07	-0,01				
4	61,92					3,5	0,2		0	0,1	0,1	0,07	-0,01		235	3,8	4,3
4,25		-16,6053	32,8954	3080		3,5	0,2	233	-0,1			0,06	0	227			

While some of the characteristics of the data presented above may be of little impact or can be easily overcome, others need a thoughtful approach as they may negatively impact the quality of the analysis performed. In the next paragraphs a description of data treatment methods is made.

3.2.2 Resampling

In order to take advantage of most data, an approach of 'upsampling' all parameters of lower sampling rate to a frequency of 4Hz is taken. Depending on the type of parameter, the perceived quality of data and the dependence of posterior analysis, different methods of interpolation are used. All interpolations are with respect to time. On Annex 1 are listed the most important parameters and the method of interpolation used, if any.

Linear interpolation is trivial and used on parameters that change slowly.

3.2.2.1 Cubic Interpolation

On parameters that present a dynamic or oscillatory behavior, a cubic spline interpolation is used. On this type of interpolation, a tridiagonal linear equation system is solved for n polynomials encompassing $n+1$ knots on the conditions that at each node the first and second derivatives of the preceding polynomial have the same values as the succeeding polynomial. That is

$$\begin{cases} q_i(x_i) = q_{i+1}(xi) \\ {q'}_i(x_i) = {q'}_{i+1}(x_i) \\ {q''}_i(x_i) = {q''}_{i+1}(x_i) \end{cases} \qquad for \;\; 1 \le i \le n-1 \tag{1}$$

The system to be solved is of the type

$$\begin{bmatrix} a_{11} & a_{12} & 0 & \cdots & \cdots & 0 \\ a_{21} & a_{22} & a_{23} & & & \vdots \\ 0 & a_{32} & a_{33} & a_{34} & & \vdots \\ \vdots & & & \ddots & & \vdots \\ \vdots & & & a_{n-1,n-2} & a_{n-1,n-1} & a_{n-1,n} \\ 0 & \cdots & \cdots & \cdots & a_{n,n-1} & a_{n,n} \end{bmatrix} \begin{bmatrix} k_0 \\ k_1 \\ \vdots \\ \vdots \\ \vdots \\ k_{n-1} \end{bmatrix} = \begin{bmatrix} b_1 \\ b_2 \\ \vdots \\ \vdots \\ \vdots \\ b_n \end{bmatrix} \tag{2}$$

where

$$\begin{aligned} a_{11} &= \frac{2}{x_1 - x_0} \\ a_{ii} &= \frac{2}{x_{i-1} - x_{i-2}} + \frac{2}{x_i - x_{i-1}} \\ a_{i,i+1} &= a_{i+1,i} = \frac{1}{x_i - x_{i-1}} \\ a_{nn} &= \frac{2}{x_{n-1} - x_{n-2}} \end{aligned} \tag{3}$$

and

$$\begin{aligned} b_1 &= 3\frac{y_1 - y_0}{(x_1 - x_0)^2} \\ b_i &= 3\left(\frac{y_{i-1} - y_{i-2}}{(x_{i-1} - x_{1-2})^2} + \frac{y_i - y_{i-1}}{(x_i - x_{i-1})^2}\right) \end{aligned} \tag{4}$$

$$b_n = 3\frac{y_{n-1} - y_{n-2}}{(x_{n-1} - x_{n-2})^2}$$

The values of k will form the terms

$$\begin{aligned} a_i &= k_{i-1}(x_i - x_{i-1}) - (y_i - y_{i-1}) \\ b_i &= -k_i(x_i - x_{i-1}) + (y_i - y_{i-1}) \end{aligned} \tag{5}$$

and these will form the multiple polynomial

$$q_i = (1-t)y_{i-1} + ty_i + t(1-t)((1-t)a_i + tb_i) \tag{6}$$

taking

$$t = \frac{x - x_{i-1}}{x_i - x_{i-1}} \tag{7}$$

3.2.2.2 Circular Cubic Interpolation

It is used in angular parameters and operates the same way as linear cubic interpolations except that the angle is first converted into the $\sin$ and $\cos$ components, interpolated and then converted back to angle.

3.2.3 Unit System homogenization and Coordinate Transformation

In order to have a coherent system of units and facilitate the application of further analysis, all the dataset is converted to SI units. In the case of the positional coordinate system (Latitude, Longitude, Altitude), it is converted to a local orthogonal isometric cartesian system with origin conveniently located on the threshold of runway 05, with x pointing East, y pointing North and z pointing up.

This conversion is made using the WGS84 ellipsoid (the same used on aircraft navigation systems) which is defined by a major semiaxis $a = 6\,378\,137\,m$ and minor semiaxis $b = 6\,356\,752\,m$.

The radius of curvature along the meridian ellipse, R, is given by

$$R = \frac{a(1-e^2)}{\sqrt{(1 - e^2(\sin\varphi)^2)^3}} \tag{8}$$

where the eccentricity is defined by

$$e = \sqrt{\frac{a^2 - b^2}{a^2}} \tag{9}$$

The radius of curvature along the first vertical, N

$$N = \frac{a}{\sqrt{1 - e^2(\sin\varphi)^2}} \tag{10}$$

Thereby, one can, for short distances, determine the cartesian coordinates in x,y,z as

$$\begin{cases} x = (N\cos\varphi)(\lambda - \lambda_{ref}) \\ y = R(\varphi - \varphi_{ref}) \\ z = z - z_{ref} \end{cases} \quad (11)$$

The values used for this airport were:

$\varphi_{ref} = 32.68994°$ $\lambda_{ref} = -16.78374°$ $z_{ref} = 44\,m$ $R = 6\,354\,041\,m$ $e = 0.08182$ $N = 6\,384\,374\,m$

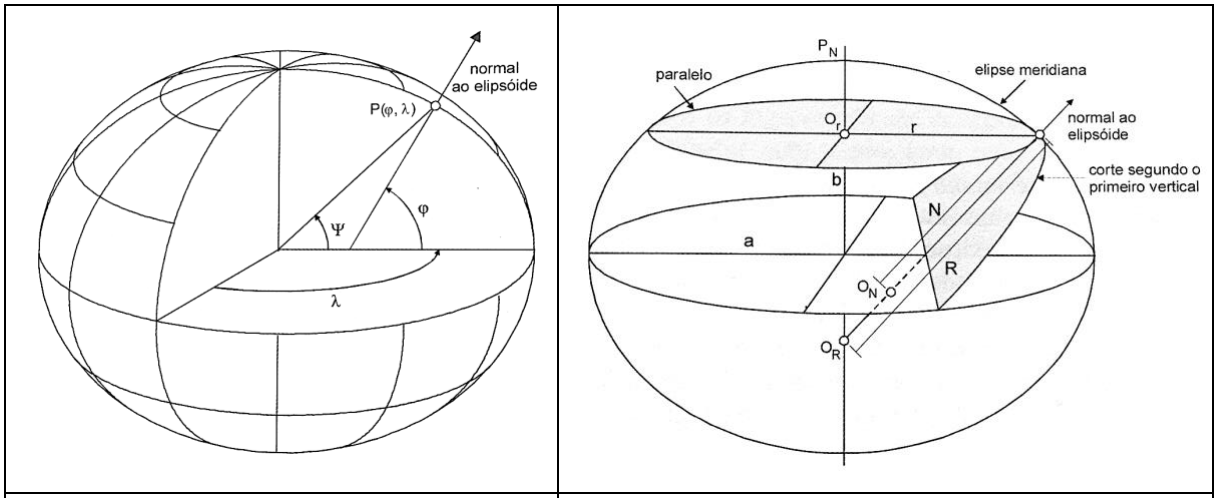

(a) (b)

Figure 3.1- (a) geographic coordinates on the ellipsoid: φ is the ellipsoidal geodesic latitude, ψ the geocentric latitude and λ ellipsoidal geodesic longitude. (b) R is the radius of curvature along the meridian and r the radius of curvature along the parallel.[29]

3.2.4 Rauch-Tung-Striebel (RTS) Smoother

The RTS smoother is used as a method to estimate the most probable state of a dynamic system and its covariance at a given time having in consideration all the measurements, both past and future. For this reason, this algorithm is only possible to implement on already existing datasets, with past and future observations, and not to real-time applications where only past observations are known.

The RTS smoother is a two-stage process: The first stage, consists of applying a Kalman filter to data in a forward-time manner, saving the filter output at each step; The second stage is a time-reverse pass whereby the algorithm incorporates its knowledge of the 'future' into 'past' measurements. In this sense, unlike low-pass filters, the RTS is able to behave optimally and not remove real variations along with noise.[30]

The Kalman filter is applied with discrete time steps ($\Delta t = 0.25\,s$) running through a prediction, measurement, and update cyclical process. The following equations in vectorial form describe the process.

Taking $\hat{\boldsymbol{x}}$ as the predicted state vector, $\boldsymbol{F}$ as the transition state function, $\boldsymbol{B}$ as the input function and $\boldsymbol{u}$ as the input vector, one can predict the state at instant t by

$$\hat{\boldsymbol{x}}_{t|t-1} = \boldsymbol{F}_t \hat{\boldsymbol{x}}_{t-1|t-1} + \boldsymbol{B}_t \boldsymbol{u}_t \tag{12}$$

The state covariance $\boldsymbol{P}$ is a function of the same parameter at the previous epoch plus the process covariance $\boldsymbol{Q}$

$$\boldsymbol{P}_{t|t-1} = \boldsymbol{F}_t \boldsymbol{P}_{t-1|t-1} \boldsymbol{F}_t^T + \boldsymbol{Q}_t \tag{13}$$

Now the prediction can be updated by the measurement $\boldsymbol{z}$, using a measurement function $\boldsymbol{H}$. For this, the residual $\boldsymbol{y}$ between the prediction and the measurement will be calculated first

$$\boldsymbol{y}_t = \boldsymbol{z}_t - \boldsymbol{H}_t \hat{\boldsymbol{x}}_{t|t-1} \tag{14}$$

the Kalman gain $\boldsymbol{K}$ is found by the next expression, where $\boldsymbol{R}$ is the measurement noise covariance

$$\boldsymbol{K}_t = \boldsymbol{P}_{t|t-1} \boldsymbol{H}_t^T (\boldsymbol{H}_t \boldsymbol{P}_{t|t-1} \boldsymbol{H}_t^T + \boldsymbol{R}_t)^{-1} \tag{15}$$

and the state vector and its covariance are updated and will be used as the starting point for the next epoch

$$\hat{\boldsymbol{x}}_{t|t} = \hat{\boldsymbol{x}}_{t|t-1} + \boldsymbol{K}_t \boldsymbol{y}_t \tag{16}$$

$$\boldsymbol{P}_{t|t} = (I - \boldsymbol{K}_t \boldsymbol{H}_t) + \boldsymbol{P}_{t|t-1} \tag{17}$$

After the Kalman filter is run, the RTS smoother will run ‘backwards’ in time.

$$\boldsymbol{P}_t^{RTS} = \boldsymbol{F}_t \boldsymbol{P}_t \boldsymbol{F}_t^T + \boldsymbol{Q}_t \tag{18}$$

$$\boldsymbol{K}_t = \boldsymbol{P}_t \boldsymbol{F}_t^T \boldsymbol{P}_t^{RTS^{-1}} \tag{19}$$

$$\hat{\boldsymbol{x}}_t = \hat{\boldsymbol{x}}_t + \boldsymbol{K}_t (\boldsymbol{x}_{t+1} - \boldsymbol{F}_t \hat{\boldsymbol{x}}_t) \tag{20}$$

$$\boldsymbol{P}_t = \boldsymbol{P}_t + \boldsymbol{K}_t (\boldsymbol{P}_{t+1} - \boldsymbol{P}_t^{RTS}) \boldsymbol{K}_t^T \tag{21}$$

The determination of the initial values for the covariance matrices $\boldsymbol{P}$, $\boldsymbol{Q}$ and $\boldsymbol{R}$ is not trivial but each has different impact on the process. $\boldsymbol{P}$ is the less sensitive and can be initialized with a rough estimate as it is updated at each epoch of the filter and quickly converges to its natural value. The selection of the values for the matrices $\boldsymbol{Q}$ and $\boldsymbol{R}$ were mainly based on existing literature on a similar problem (see [30], [9], [31]) and additionally some trial and error was needed. The choice of initial values for these matrices can be found on Annex 2.

The use of the RTS filter smoother allows for several sources of data to be incorporated in the best estimation of the parameters through the manipulation of the measurement function $\boldsymbol{H}$ and the noise covariance of the measurements, $\boldsymbol{R}$. In this case, a mix of Inertial, barometric and GPS data was used for the estimation of Position, Velocity and Acceleration, all in x, y, and z.

An additional advantage is that the extracted parameters tend to converge to a state of coherence among themselves as they are related with each other through the transition state function $\boldsymbol{F}$ and after the update step, sensor bias tends to be cancelled out for the next iteration.

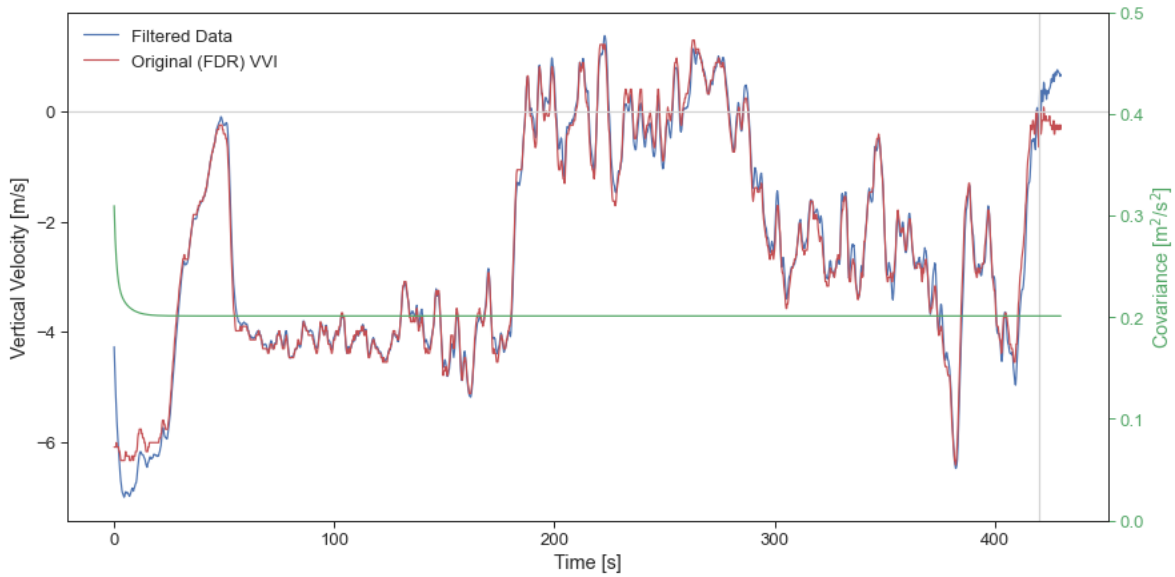

Figure 3.2 - A sample of Vertical Velocity data from a flight. After the first few iterations the filtered data converges with measured data and the covariance stabilizes and maintains constant throughout the process. The vertical line at 420 s corresponds to the moment of landing.

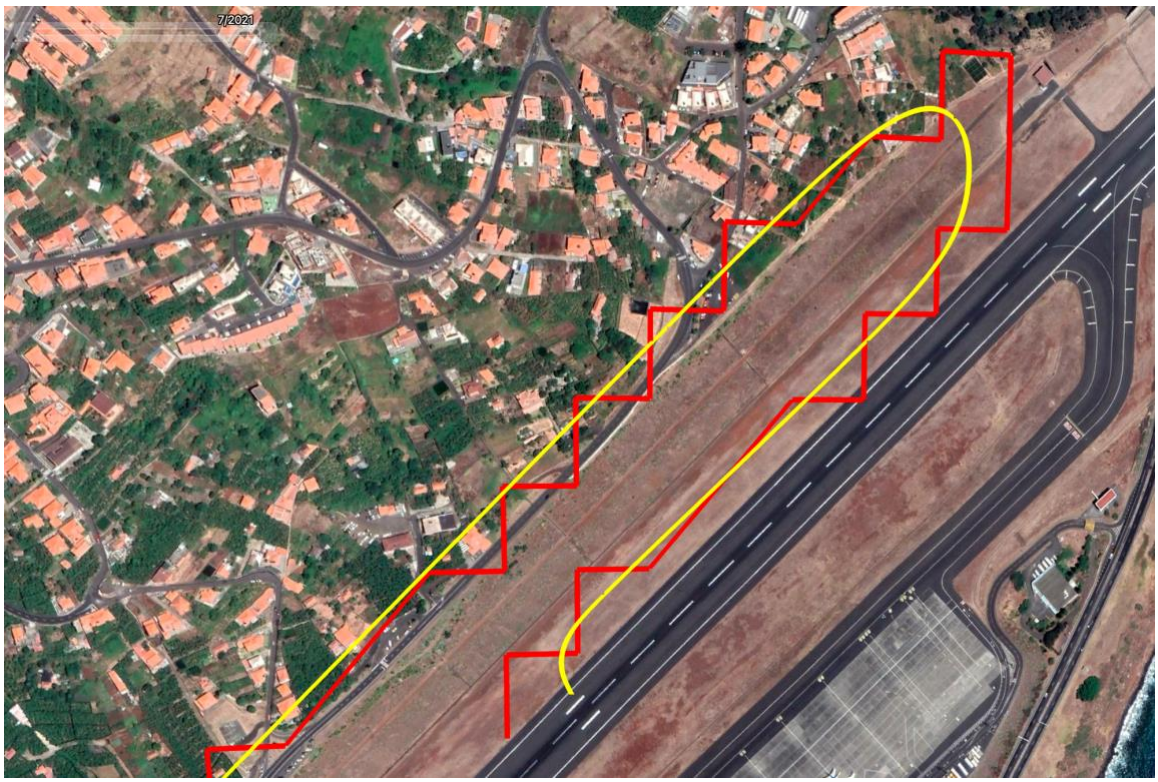

Figure 3.3 - Flight trajectory before (red) and after (yellow) application of the RTS smoother. Note that there is still a shift to be corrected.

3.2.5 Trajectory shift / adjustment

Due to imprecision on aircraft navigation system and/or difference of datum the geospatial data evidenced dispersion among samples and some degree of offset from the runway as depicted on Google Earth® which was used as a geospatial visualization tool. In order to keep a coherence among the geospatial data this offset was corrected by shifting the flight path data so that it is made to intersect two conveniently selected points, one on the runway centerline and other on the exit taxiway. In this manner the trajectory is corrected laterally and longitudinally relative to the runway – See Figure 3.4.

The method used can be summarized the following way:

1. The touchdown time is detected on the data for a particular flight
2. The offset ($\Delta x, \Delta y$) between the aircraft at that moment and a conveniently selected touchdown point located on the runway centerline is determined.
3. That offset is subtracted to all the positional data for that flight.
    a. At this stage, the trajectory is aligned with runway centerline but still has offset in the longitudinal direction.

As all the flights leave the runaway via the same taxiway, that position can be used as anchor point to determine the longitudinal (as referenced to the runway) offset.

4. The intersection of a line passing on the taxiway anchor point and parallel to the runway with the path of the flight is determined and an offset is calculated.
5. The flight path data is adjusted correspondingly, by subtracting the offset to all positional data.

On the vertical axis, although the errors were found to be of little magnitude, the trajectory is also shifted.

Once the horizontal offsets are applied, it is recovered where, along the runway, did the touchdown take place. This is important because the runway has an upslope of 0,8% until 200m after the touchdown point and 1,0% thereafter, until 1100m. So, the altitude of touchdown increases along the runway.

Once the touch down vertical offset is determined, that correction is applied to all altitudes.

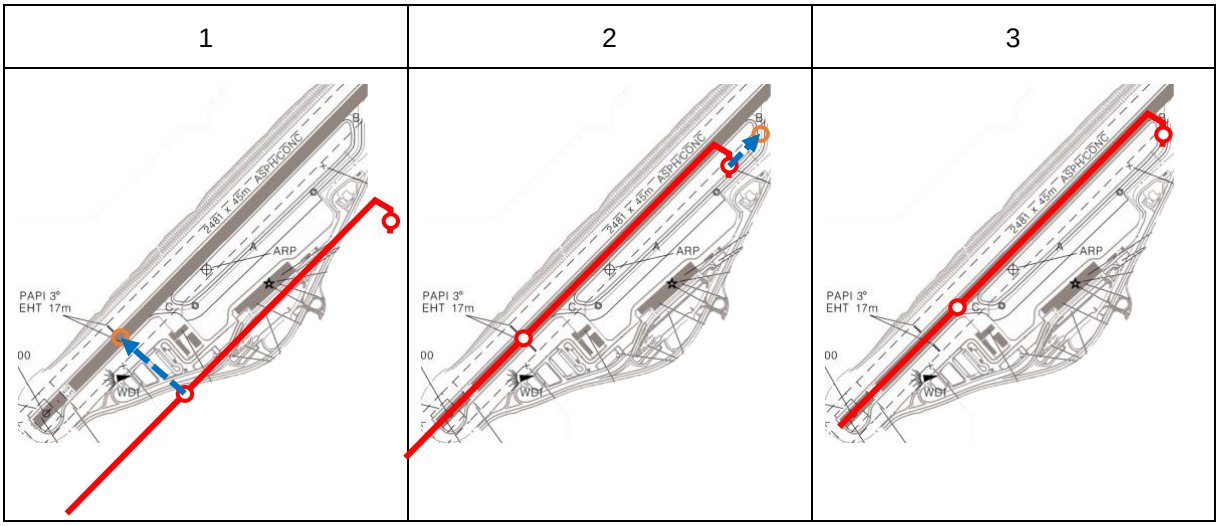

Figure 3.4 - Trajectory adjustment scheme.

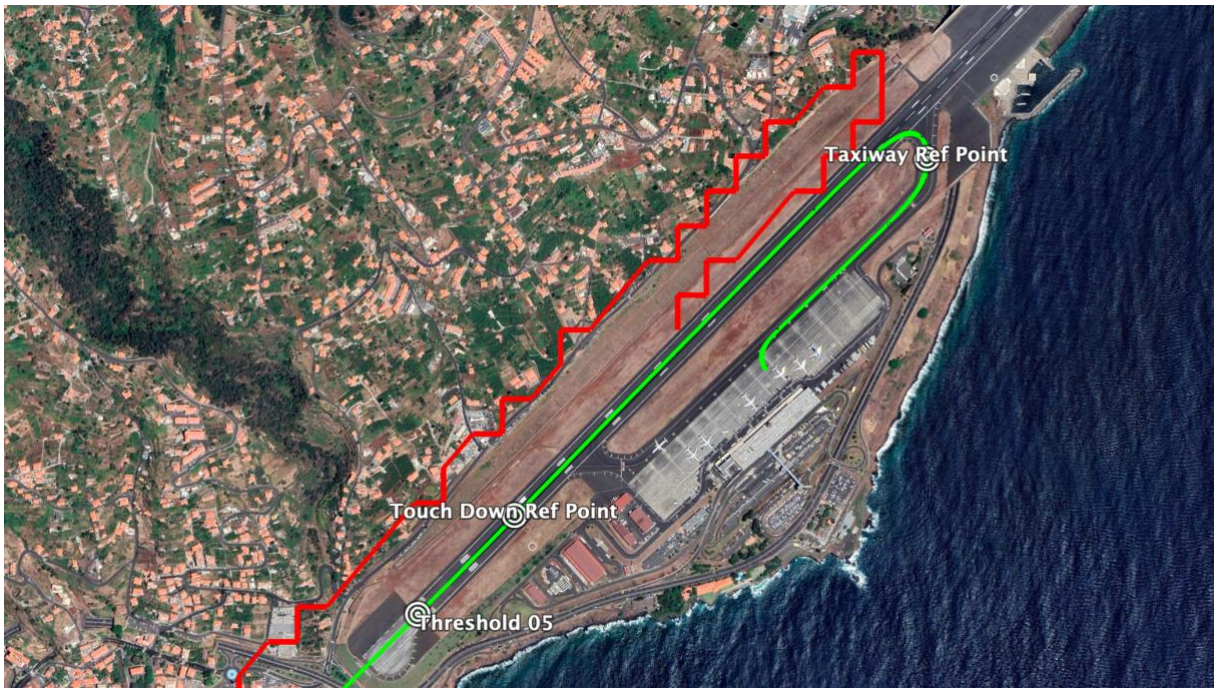

Figure 3.5 – In green an example of the horizontal projection of the flight path after RTS smoothing and adjustment. The points referenced are used for Local Coordinate System origin (Threshold 05) and trajectory shifting (Touchdown and Taxiway)[Image source: Google Earth®].

4 Data analysis

4.1 Axes System

For analysis coherence, the axes system needs to be chosen and implemented accordingly, although on many instances, when depicting the data on charts or tables, the signs are adjusted so that its interpretation is more intuitive e.g. altitudes increase positively when going up instead of positive downwards as some axes system use.

4.1.1 Earth Frame

Orthogonal, right handed, origin on the center of the earth. Usually used in polar format, as Latitude, Longitude and Altitude.

4.1.2 Local Earth Frame [i]

Orthogonal, right handed with origin conveniently located at a point, generally on the surface of the ellipsoid. In this work, the origin for this frame is on the runway 05 threshold.

Axis orientation and positive directions are:

- x to the East, tangent to the ellipsoid;
- y to the North, tangent to the ellipsoid;
- z upward, away from the center of the earth.

For practical purposes this frame can be regarded as an inertial frame.

4.1.2.1 Runway Frame

Same as Local Earth frame but the x, y axes rotated about z so that y is along the runway centerline and x is perpendicular to the runway centerline.

4.1.3 Body Frame [b]

Orthogonal, right handed, with origin on aircraft CG. Linear forces, velocities and accelerations positive directions are:

- x is forward, along the fuselage;
- y is to the right wing;
- z is downward.

Rotational velocities, accelerations and moments are positive in the clockwise direction as seen from the origin looking along the positive axis. E.g.

- pitch up
- roll right
- yaw right

4.1.3.1 *Stability Frame*

A rotation of the body frame around the y axis so that the x axis is now along the projection of the velocity vector on (x,z) plane.

4.1.4 Air Mass Frame (wind) [a]

Orthogonal right handed, with origin on the aircraft CG and positive directions as follows:

- x forward along the air-relative velocity vector
- y on the parallel to the plane of the wings, to the right
- z orthogonal to (x,y) pointing down

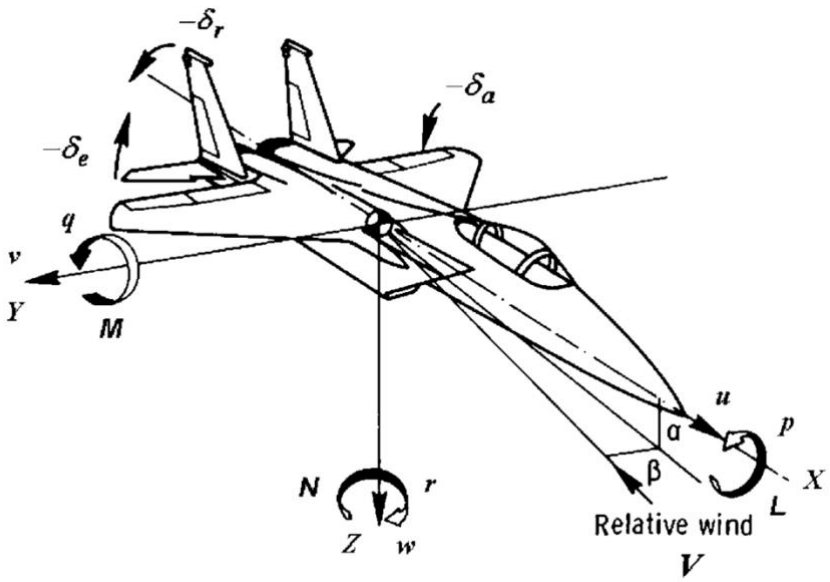

Figure 4.1 - Aircraft axes notation and sign convention.[32]

4.2 3D Wind Estimation

A tridimensional wind estimation is not computed on board the aircraft - only horizontal components are. But it is important to know the vertical component of the wind in order to calculate parameters such as turbulence and wind shear metrics. The wind vector can be deduced from QAR data, albeit not rigorously, due to sensor inaccuracies and general lack of precision - the WMO on its *Aircraft Meteorological Data Relay Reference Manual*[15] makes an estimation that at typical approach speeds, an error of at least 1 m/s should be expected. But using the data after RTS smoothing may provide for a somewhat better basis for calculation.

A method of estimating the complete wind vector can be implemented by realizing that the wind is the difference between the aircraft inertial velocity and its velocity relative to the air mass.

$$\boldsymbol{V}_{ai} = \boldsymbol{V}_{bi} - [\boldsymbol{T}_{ib}] \cdot \boldsymbol{V}_{ab} \tag{22}$$

The body velocity relative to the inertial frame expressed in inertial coordinates V_{bi} was already computed in the RTS smoother. The velocity relative to air mass expressed in body frame is

$$\boldsymbol{V}_{ab} = \begin{bmatrix} V_a \cos\alpha \cos\beta \\ V_a \cos\alpha \sin\beta \\ V_a \sin\alpha \end{bmatrix} \tag{23}$$

Where V_a is the velocity relative to the air expressed in wind axes, available in the FDR as True Airspeed.

Generically, these transformation matrices can be used to translate to and from different reference frames, through Euler angles:

$$\boldsymbol{T}_{ba} = \begin{bmatrix} c\alpha c\beta & -c\alpha s\beta & -s\alpha \\ s\beta & c\beta & 0 \\ s\alpha c\beta & -s\alpha s\beta & c\alpha \end{bmatrix} \tag{24}$$

$$\boldsymbol{T}_{ib} = \begin{bmatrix} c\psi c\theta & c\psi s\theta s\phi - s\psi c\phi & c\psi s\theta c\phi + s\psi s\theta \\ s\psi c\theta & s\psi s\theta s\phi + c\psi c\phi & s\psi s\theta c\phi - c\psi s\phi \\ -s\theta & c\theta s\phi & c\theta c\phi \end{bmatrix} \tag{25}$$

Where $c\alpha$ and $s\alpha$ are a condensed representation of the $\cos\alpha$ and $\sin\alpha$, respectively.

It is apparent from these expressions that correct angles in body axis frame are paramount for correct calculations. The body angles ψ, θ and ϕ are available on QAR data and have been subject to smoothing as described in 3.2.4. The sideslip β is not on available on QAR although it can be estimated from the record of lateral accelerations, as presented further ahead on section 4.2.2. The Angle of Attack, α is available in the data, but it is known that these values need a calibration before use as they present bias and scaling errors.[8], [11]

4.2.1 Angle of Attack Calibration

The aircraft has 3 AOA probes (#1 and #3 on the left side of the fuselage, #2 on the right side). Of these only the data of #1 and #2 was available. The fact that the probes are in the forward section of the fuselage affects the measurements when the aircraft is rotating about its y axis (pitching).

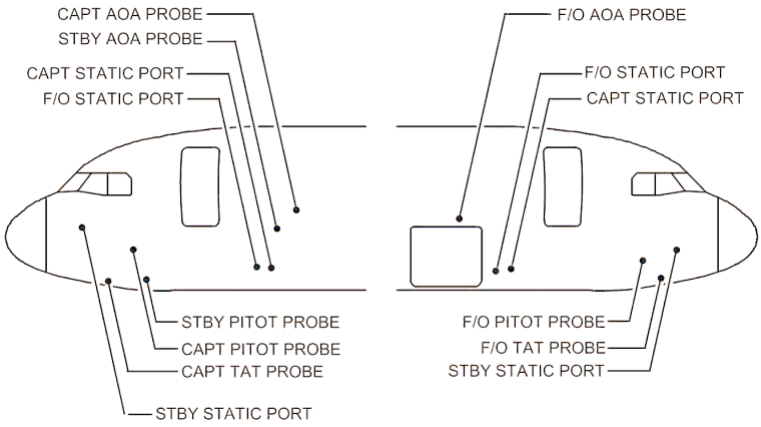

Figure 4.2 - Location of probes on the aircraft fuselage.

The method of correction proposed is through the relation [11]:

$$\frac{\theta - \gamma}{\cos\phi} = k\left(\frac{AOAL + AOAR}{2} - \frac{Lq}{V_a}\right) + c \tag{26}$$

Where $AOAL$ and $AOAR$ are the values on the QAR of the left and right AOA probes, q is the pitch rate and V_a is the true air speed.

L is the arm length from the center of gravity of the aircraft to the AOA probes and has the following values for the aircraft concerned:

A319: 6.88 m

A320: 8.48 m

A321: 12.75 m

The constants k and c are the resultant of a least squares fit of the above expression over a flight data.

From Figure 4.3 it can be observed that a reasonably good correlation can be achieved for the most part of the flights. As could intuitively be expected, lower mean wind intensities and lower deviations from mean are more conducive to higher AOA regression correlation as both these conditions are associated with less disturbance on the flight.

Inherent to this method of AOA correction is the assumption that the integral of the wind's vertical component throughout the considered flight path is zero. Please note that θ, ϕ and most notably γ, the flight path angle, are expressed in the earth frame. γ usually defined by

$$= \tan^{-1}\frac{V_{z,bi}}{|V|_{bi}} \tag{27}$$

Where the subscript $_{bi}$ represents the body relative to earth frame.

But the AOA, α, which is meant to be represented in equation (26) by $\frac{\theta-\gamma}{\cos\phi}$ is relative to the air mass. So, generally any wind will give rise to an error. To correct this one can substitute $|V|_{bi}$ by $|V|_{ba}$, which

is to a good approximation the True Air Speed and eliminate the error of the horizontal components of wind. But this method can not be done for the vertical wind component as it is unknown.

For this reason, and because it is assumed that the vertical component of wind is generally small, the regression described above is made over a large distance where it is assumed that the updrafts and downdrafts cancel out.

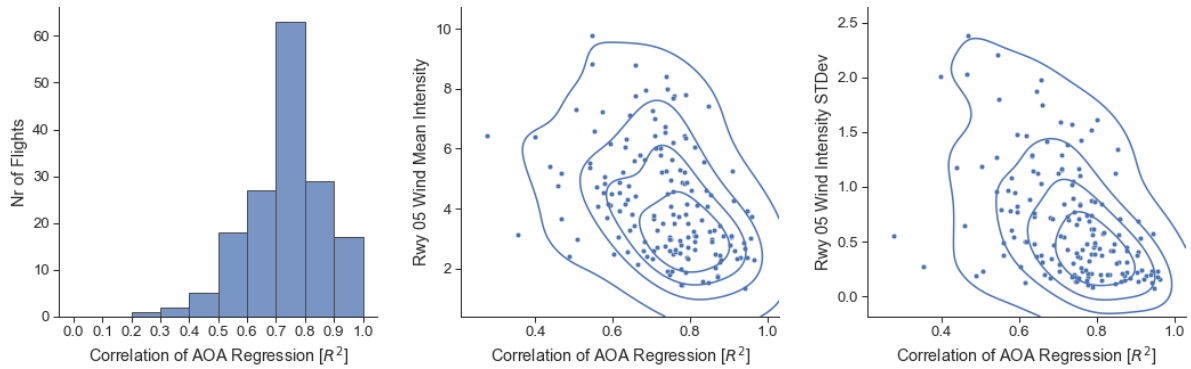

(a) (b) (c)

Figure 4.3 - Correlation of the AOA Least Squares Fit for all the considered flights.

4.2.2 Sideslip angle estimation

The aircraft is not equipped with sensors and therefore the QAR does not record the sideslip angle β. The proxy measure used to estimate β is the lateral acceleration and a method by which this can be done has been suggested by Haverdings and Chan [16]. This method, with adaptations, recognizes that on a sideslip there are two major contributors to side forces: the vertical fin and the fuselage.

$$Y = Y_{vfin} + Y_{fus} \tag{28}$$

Where the vertical fin is taken as a semi-wing of symmetrical profile which generates a lift given by

$$Y_{vfin} = \frac{1}{2}\rho S_{vfin} V^2 \frac{\partial C_{L_{fin}}}{\partial \beta}\beta \tag{29}$$

For the vertical fin, assuming a symmetrical airfoil (eg. NACA 0007) with a $C_{l_\alpha}$of 5.73/rad one can deduce the 3d C_{L_α} with the empirical expression proposed by Lowry and Polhamus [33] for uncompressible flow which is adequate since the Mach number at approach speed is $M < 0.2$:

$$C_{L_\alpha} = \frac{C_{l_\alpha} A}{\frac{C_{l_\alpha}}{\pi} + \sqrt{\left(\frac{A}{\cos\Lambda}\right)^2 + \left(\frac{C_{l_\alpha}}{\pi}\right)^2}} \tag{30}$$

Plugging in the values for A≈6.5 and Λ=27,5°, C_{L_α} (which in this case becomes, C_{L_β}) comes out as 3,98/rad.

Assuming the fuselage as a slender cylindrical body, and decomposing the side slip flow into longitudinal and transversal components, according to Jones [34], the expected C_D for the cross flow is on the order of 0.6, for a Reynolds number of

$$Re_{fusXflow} = \frac{\rho D_{fus} V \sin\beta}{\mu} = \frac{1.225 \cdot 3.95 \cdot 75 \cdot \sin 3°}{18.5 \times 10^{-6}} = 1.03 \times 10^{6} \tag{31}$$

For sea-level ISA conditions, taking the fuselage diameter as reference and 3° of sideslip.

So, the side force produced by the fuselage, linearizing $\sin\beta \approx \beta$ for small angles, would be given by

$$Y_{fus} = \frac{1}{2}\rho S_{fus} C_{D_{fus}} (V\beta)^2 \tag{32}$$

Substituting equation (29) and (32) into (28) and solving for β, one gets

$$S_{fus} C_{D_{fus}} \beta^2 + S_{vfin} \frac{\partial C_{l_{fin}}}{\partial \beta} \beta - \frac{Y}{Q} = 0 \tag{33}$$

At this point one would be suggested to neglect the β^2 (fuselage) term as for small β that becomes even smaller, nevertheless on reference [16], Haverdings and Chan advise not to do so. In fact on Figure 4.4 it can be seen that for larger values of β (around 10°) the contribution of the fuselage side forces can be 15% of the total force and it is not clear to the author at this time if that proportion is not greater in reality.

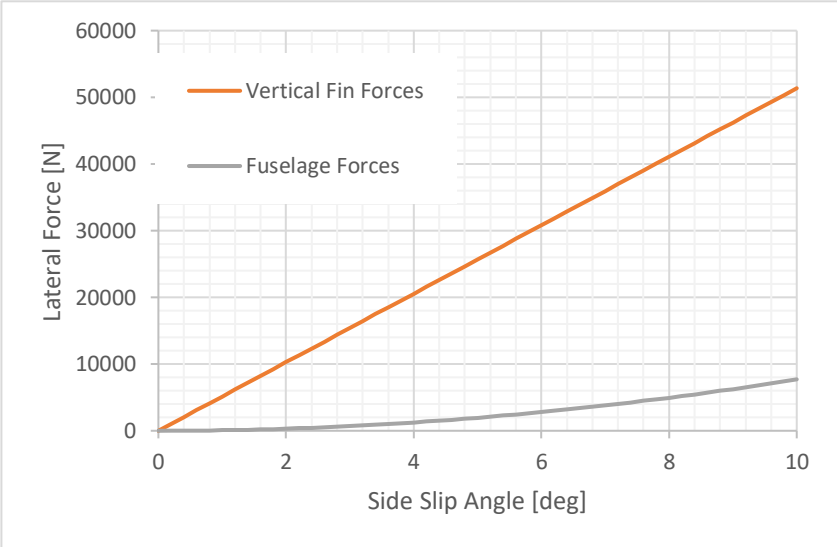

Figure 4.4 – Contribution to lateral forces during side slip.

Solving equation (33) in order to β and knowing that $Y = ma_y$ one gets

$$\beta = \frac{-S_{vfin}\frac{\partial C_{L_{fin}}}{\partial \beta} \pm \sqrt{(S_{vfin}\frac{\partial C_{L_{fin}}}{\partial \beta})^2 - 4(S_{fus}C_{D_{fus}})(-\frac{ma_y}{Q})}}{2S_{fus}C_{D_{fus}}} \tag{34}$$

Sideslip angle β can thus be estimated through the lateral acceleration a_y.

The fuselage surface for the purpose of this formula is taken simply as the longitudinal cross-sectional area, that is, $L \times D$. Since this is a rough estimate, the length of the fuselage may be taken as the total length as depicted on Figure 2.6.

4.2.3 Model validation

Although there is no information about the wind affecting the aircraft other than that derived by the aircraft systems themselves, it can nevertheless be verified if the method of filtering and processing the data produces results that are in general agreement with aircraft sensors. On Figure 4.5 it can be observed that the computed wind values generally follow in trend and magnitude the real-time on-board sensed values that were recorded on the QAR.

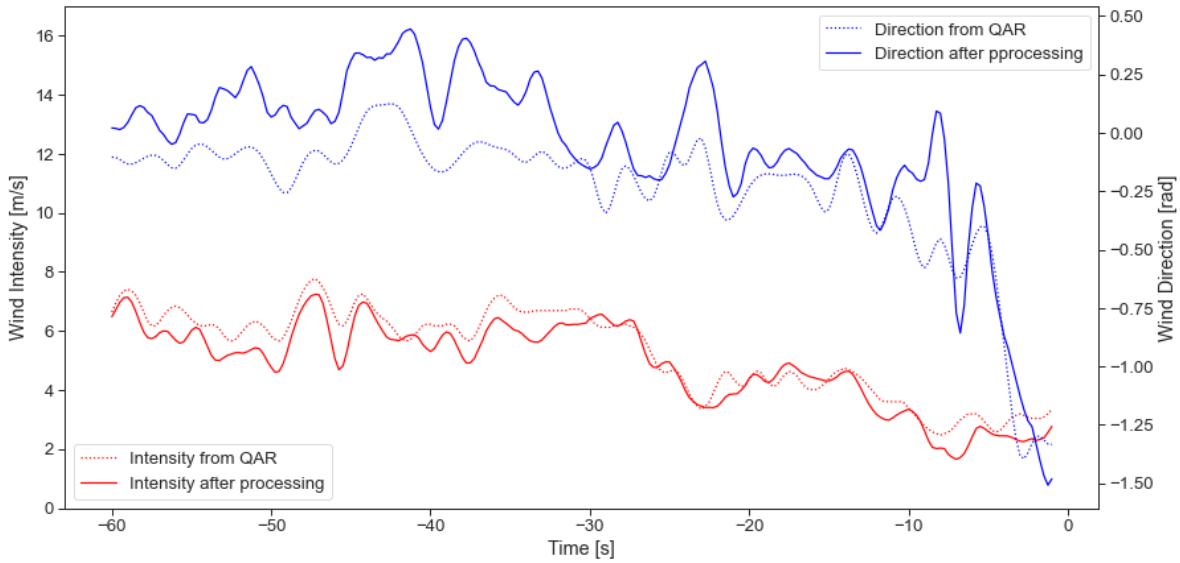

Figure 4.5 - Sample of wind values for a particular flight as recorded by the aircraft systems and after data processing.

4.2.4 Wind Categorization

It must be emphasized that although the 2 minute mean wind intensity is taken as reference in accordance with wind reporting standards by ICAO and WMO, that period can in reality contain great variations both in direction and intensity, including short lived gusts that may fall between anemometer records. Wind behavior studies by Wieringa[35] shows that the gustiness may be attributable to many phenomena but for a given measuring site, considering the roughness of surrounding terrain and the wavelength of the gusts, a near linear relation can be established with mean wind intensity. Such linearity may also be observed on Figure 4.6.(a) which shows a positive correlation between the gusts and the mean intensity for the flights being considered. Generally, the intensity varies between 0.6 and 1.4 of the mean value while the direction varies between ±40º (see Figure 4.6 (b)). Additionally, on the same study, Wieringa notes that small scale wind fluctuations (spatial or temporal) have negligible correlation in locations further away than 100 m downwind or 50 m crosswind from the observation point.

Only mean intensity and general gustiness, when averaged over a sufficiently long period, are correlatable. This underlines the inherent stochastic nature of wind and the fact that near the surface, it is dominated by turbulent phenomena.

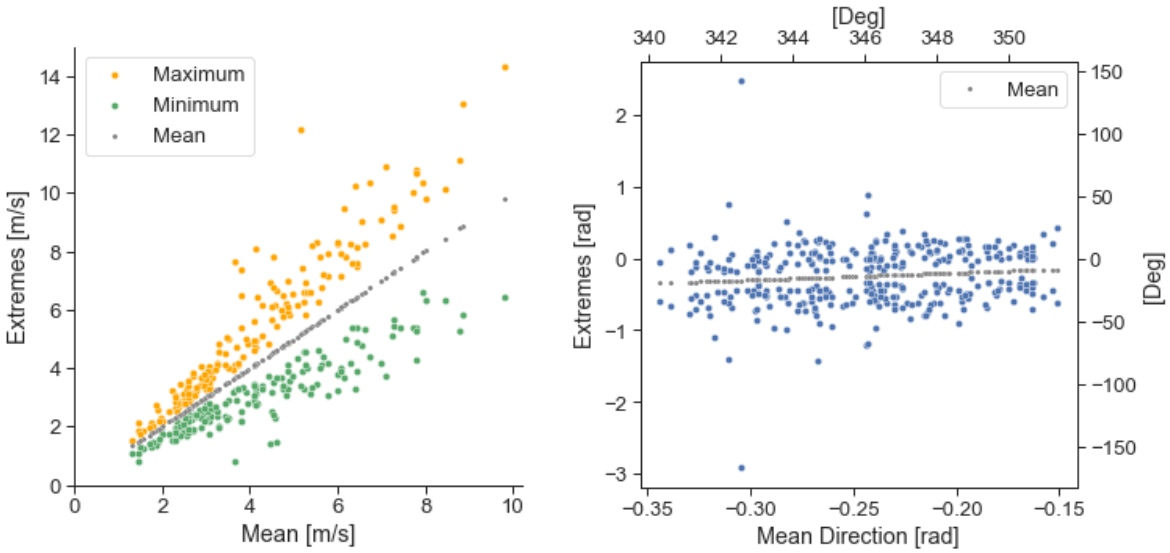

(a) (b)

Figure 4.6 – (a) Maximum and minimum of the wind intensity during the 2 minutes before touchdown, for each flight. (b) Maximum and minimum directions of the same samples.

For this reason, as will be seen ahead, it is difficult to find a direct correlation between specific aircraft flight perturbations and individual surface wind variations, but rather a general connection between mean surface wind intensity and gustiness and mean aircraft reaction. This would suggest the use of two discriminatory elements – mean intensity and gustiness – for the analysis of aircraft behavior. But Figure 4.7 shows that there is a reasonably good direct correlation between these parameters, which, for simplicity, allows the use of a single one serving as a proxy for the other. For convenience, the mean intensity is chosen.

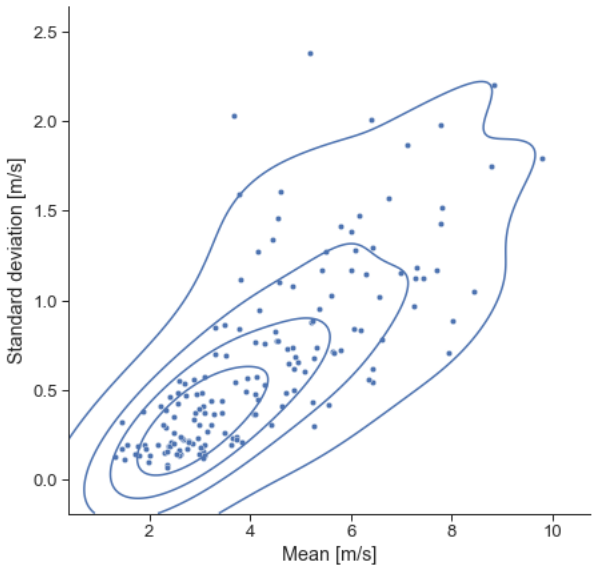

Figure 4.7 - Runway 05 Anemometer correlation between the Mean and the Standard Deviation of Intensity for the flights analyzed.

It was selected to conduct the analysis of the aircraft parameters during the approach by using a division into 4 classes of surface wind. These are based on the 2 minute mean intensity at the Rwy 05 anemometer. The division of the classes is chosen so to keep a tractable number of situations but with special attention to have smaller bins on wind regimes that cause most operational disturbance.

These are:

Table 2 - Wind intensity Classes

Wind Class	Lower bound	Higher bound	# Samples
1	0 m/s	4 m/s	86
	0 kts	7.8 kts	
2	4 m/s	5.5 m/s	38
	7.8 kts	10.7 kts	
3	5.5 m/s	7 m/s	23
	10.7 kts	13.6 kts	
4	> 7 m/s	-	15
	> 13.6 kts	-	

4.2.5 3D Wind Component results

Figure 4.8 depicts the mean wind components felt during the last 1800m (about 1 nm) of the approach for the 4 classes of surface wind.

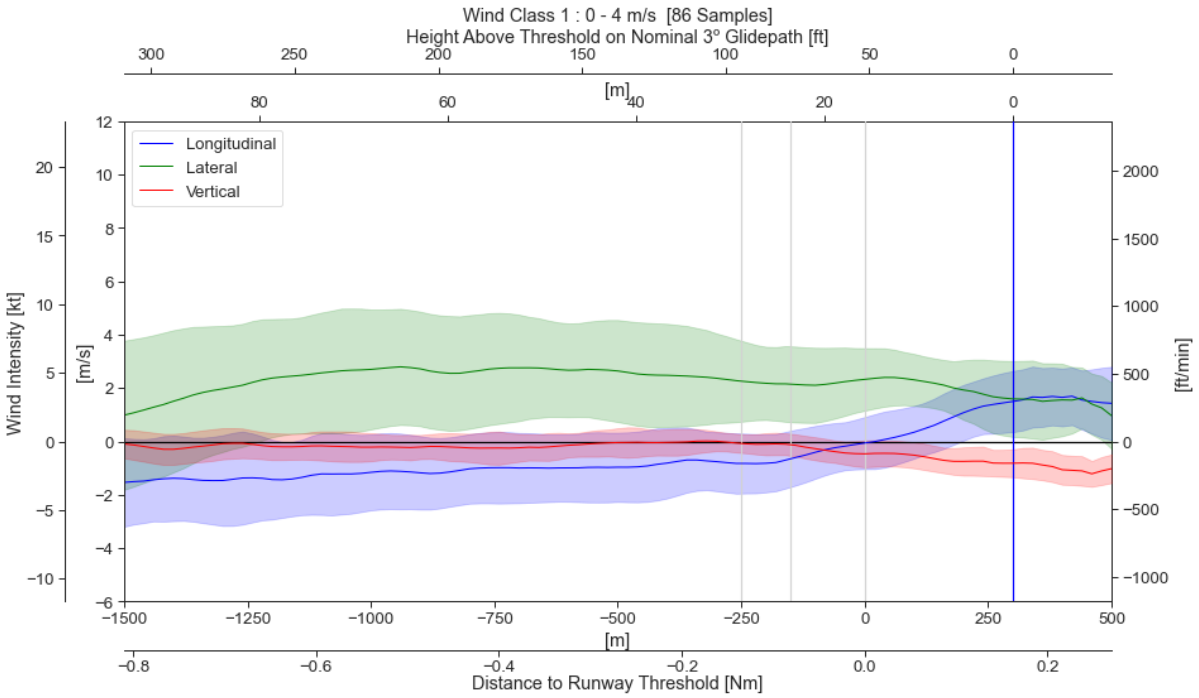
Wind Class 1 : 0 - 4 m/s [86 Samples]
Height Above Threshold on Nominal 3° Glidepath [ft]
Longitudinal
Lateral
Vertical
Wind Intensity [kt]
[m/s]
[ft/min]
[m]
Distance to Runway Threshold [Nm]

(a)

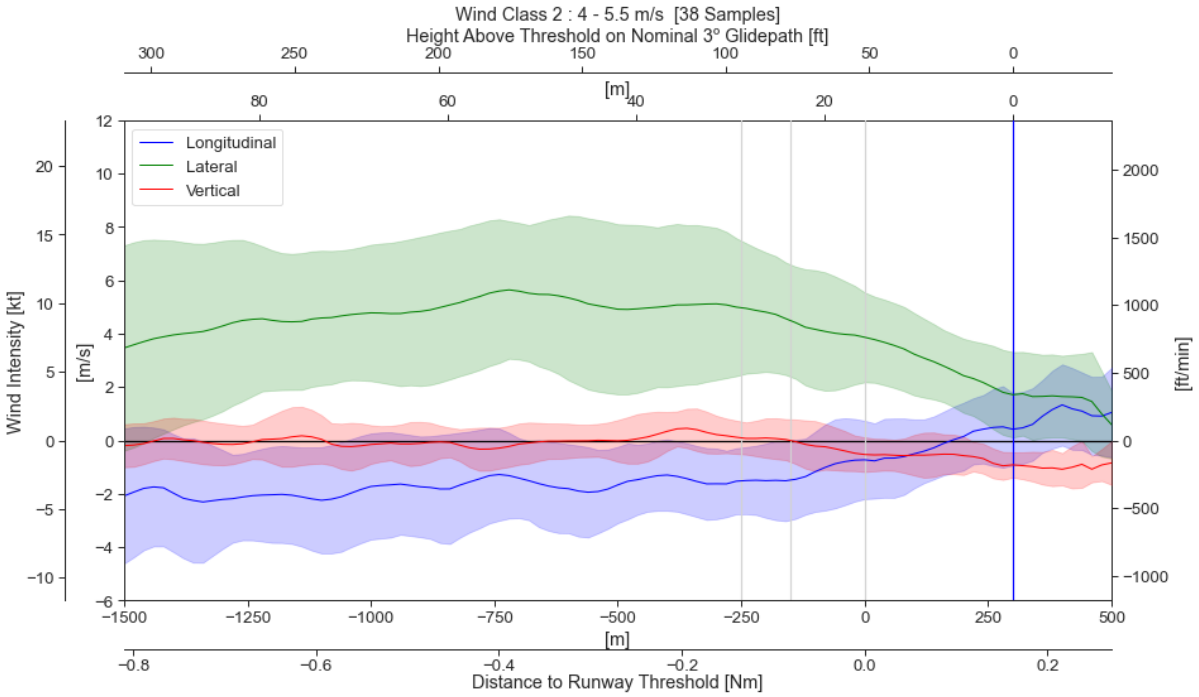
Wind Class 2 : 4 - 5.5 m/s [38 Samples]
Height Above Threshold on Nominal 3° Glidepath [ft]
Longitudinal
Lateral
Vertical
Wind Intensity [kt]
[m/s]
[ft/min]
[m]
Distance to Runway Threshold [Nm]

(b)

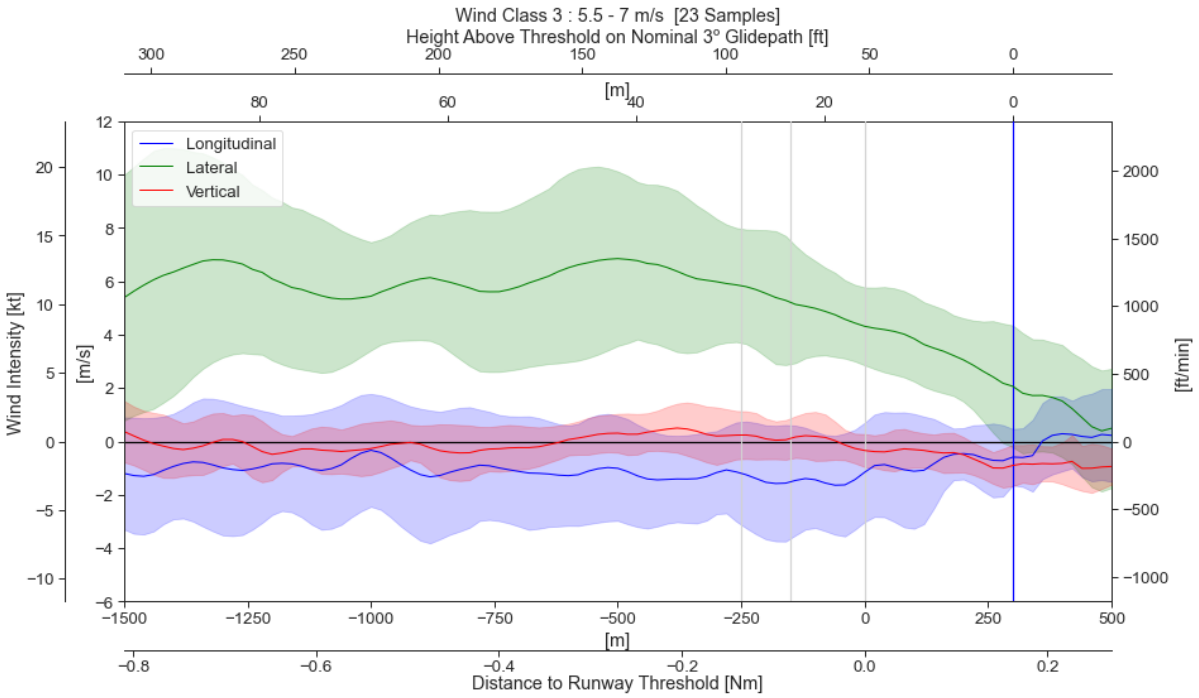

(c)

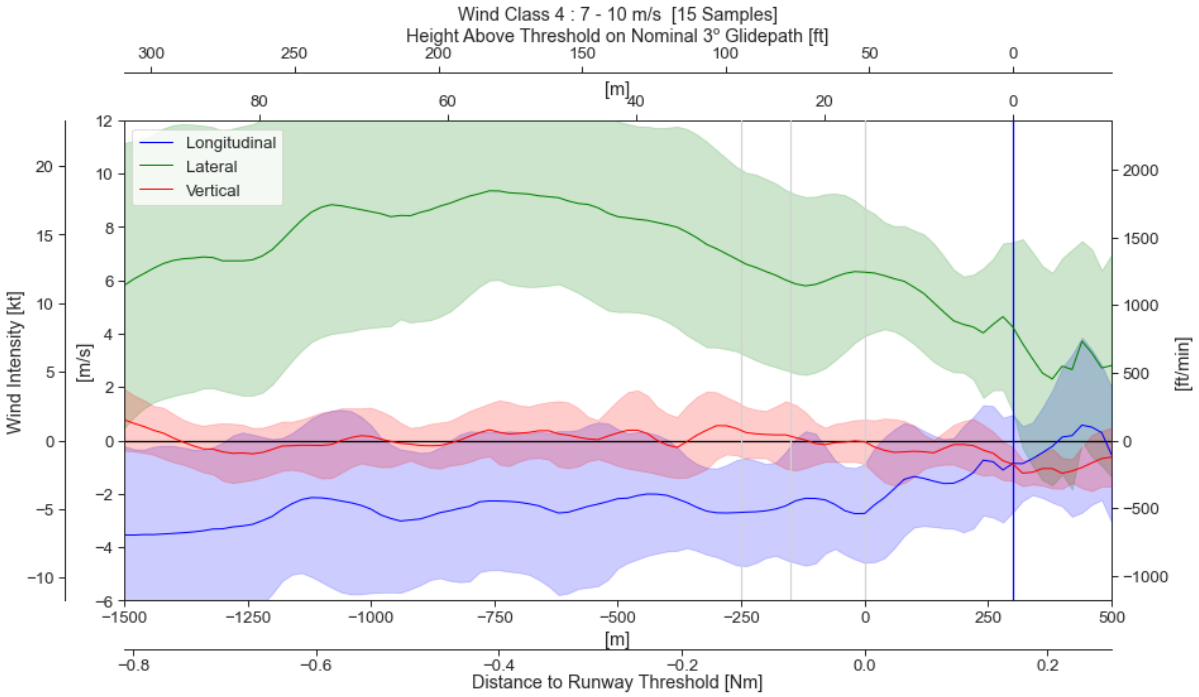

(d)

Figure 4.8 - Mean wind components for each class. Shaded areas represent a Standard Deviation. Positive directions are forward, right and up.

Remarks on the interpretation of these graphics:

- Vertical lines mark the position of notable orographic points. See Figure 4.9 for additional reference.
    - -250 m – Transition from sea to land; start of terrain slope to runway height;
    - -150 m – End of slope to runway height; start of flat terrain;
    - 0 m – Runway threshold;
    - +300 m – Blue line; Start of touchdown zone; point of interception of nominal glideslope with runway.
- The shaded areas represent a Standard Deviation from the mean of samples of that wind class.
- The positive directions of the longitudinal, lateral and vertical components are forward, right and up, respectively.
- Past the 300 m mark (touchdown point), the statistics must be taken with reservation or disregarded as the number of samples reduces rapidly with distance. The reason is that flights are removed from the sampling as touchdown is detected.

Figure 4.9 - Distance reference markers [Base image © Google Earth]

4.2.6 Conclusions from the analysis of 3D wind components

Overall, the wind components extracted after the calculations show mainly a stochastic behavior which can be appreciated by the wide bands of the standard deviation which increase proportionally to the wind intensity. As the wind direction being studied is 60º from the left of the flightpath, it is normal that the crosswind has the highest component and standard deviation, followed by the headwind component and finally the vertical component which remains around 0.

Nevertheless, it can be observed that for lower wind intensities (class 1 and 2) upon crossing the end of the orographic slope from the sea to the runway plateau, there is a decrease of headwind, eventually becoming tailwind, accompanied by a small downdraft. On higher wind intensities (class 3 and 4) this effect manifests itself slightly ahead, closer to the runway threshold, albeit with similar magnitude.

For all wind classes the crosswind exhibits its maximum between -800 m and -500 m, then reducing progressively until touchdown, except for class 4, where a trend inversion is felt momentarily just before crossing the threshold. This crosswind reduction is significant as it forces the pilot to correct the lateral axis by using bank on a late stage and may unstabilize the approach laterally. An appreciation of bank angles can be found on 4.3.3.1.

Although these average patterns may be observed, it is never enough to stress that each individual flight may diverge significantly from these as the wind varies in a random fashion.

Additionally, it was observed after charting the data of the aircraft path on final that there is a significant geospatial dispersion up until 500 m distance from threshold. This means that even for exact same surface wind conditions, two aircraft on slightly different paths may observe different local winds.

Figure 4.10 - Geospatial dispersion of Flights analyzed. [Base image © Google Earth]

4.3 Analysis of flight perturbations on final

4.3.1 Turbulence metrics

There are multiple turbulence metrics in use today for aircraft. The simplest expression of turbulence can be measured by the variation of vertical acceleration felt onboard, although this is not a measure of turbulence in itself but rather the effects of it. The vertical acceleration is a function of several factors, namely the weight, velocity, altitude and the nature of the turbulence, making this metric very aircraft-specific. Furthermore, it might be difficult to decouple the intentional aircraft maneuver from the external turbulent inputs.

In terms of meteorological reporting, other metrics, more aircraft-independent, are preferred, such as the EDR (Eddy dissipation Rate) and the DEVG (Derived Equivalent Vertical Gust), but in the particular case of this analysis, since the aircraft are of the same type, hence very similar in-flight characteristics, is seems adequate to use the metric of vertical acceleration to quantify and compare

the disturbances among them. Also, it must noted that these are the effects really felt by the aircraft and its occupants.

4.3.1.1 Vertical Acceleration Turbulence Metric

For the classification of turbulence according to this metric, the table proposed on reference [15] may be used.

Table 3 - Turbulence categorization based on vertical acceleration [15]

Turbulence category	Peak Acceleration (Δn)
None	$\lvert\Delta n\rvert < 0.15$ g
Light	$0.15\ g \leq \lvert\Delta n\rvert < 0.5\ g$
Moderate	$0.5\ g \leq \lvert\Delta n\rvert < 1.0\ g$
Severe	$\lvert\Delta n\rvert \geq 1.0$ g

From Figure 4.11 below it can be observed that effectively the vertical acceleration amplitude, hence turbulence, increases with higher wind classes, as expected.

Normally, for all wind classes, the turbulence maintains on the '*light*' area but it must be noted that at this stage, the aircraft are flying at a speed of approximately $1.3 \cdot V_S$, so the maximum load factor possible is on the order of $1.3^2 \approx 1.7$, that is, a $|\Delta n|$ of 0.7. Reaching a Δn of 0.5 (moderate turbulence category) would mean at this late stage of the approach, not only a situation dangerously close to stall but also would imply a change in vertical trajectory that most probably would prompt the pilot to initiate a Go-Around maneuver.

All the data analyzed is of aircraft that have landed, and as such is natural that an increase of the mean load factor is observed from around the mark of -100m until the +300m (touchdown point) due to the 'flare' maneuver, that is, the action where the pilot arrests the rate of descent (which would be on the order of 3.8 m/s) to nearly zero, for smooth landing.

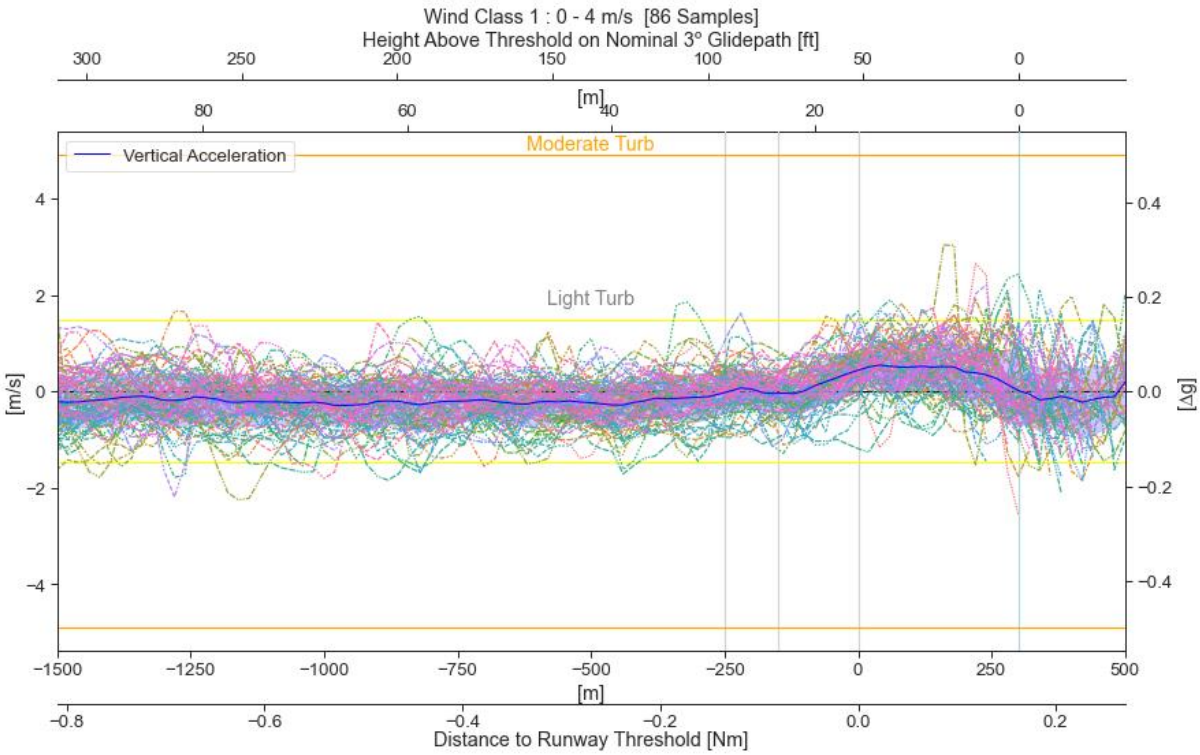
Wind Class 1 : 0 - 4 m/s [86 Samples]
Height Above Threshold on Nominal 3° Glidepath [ft]
300
250
200
150
100
50
0
[m]
80
60
40
20
0
Vertical Acceleration
Moderate Turb
Light Turb
4
2
0
−2
−4
[m/s]
0.4
0.2
0.0
−0.2
−0.4
[Δg]
−1500
−1250
−1000
−750
−500
−250
0
250
500
[m]
−0.8
−0.6
−0.4
−0.2
0.0
0.2
Distance to Runway Threshold [Nm]

(a)

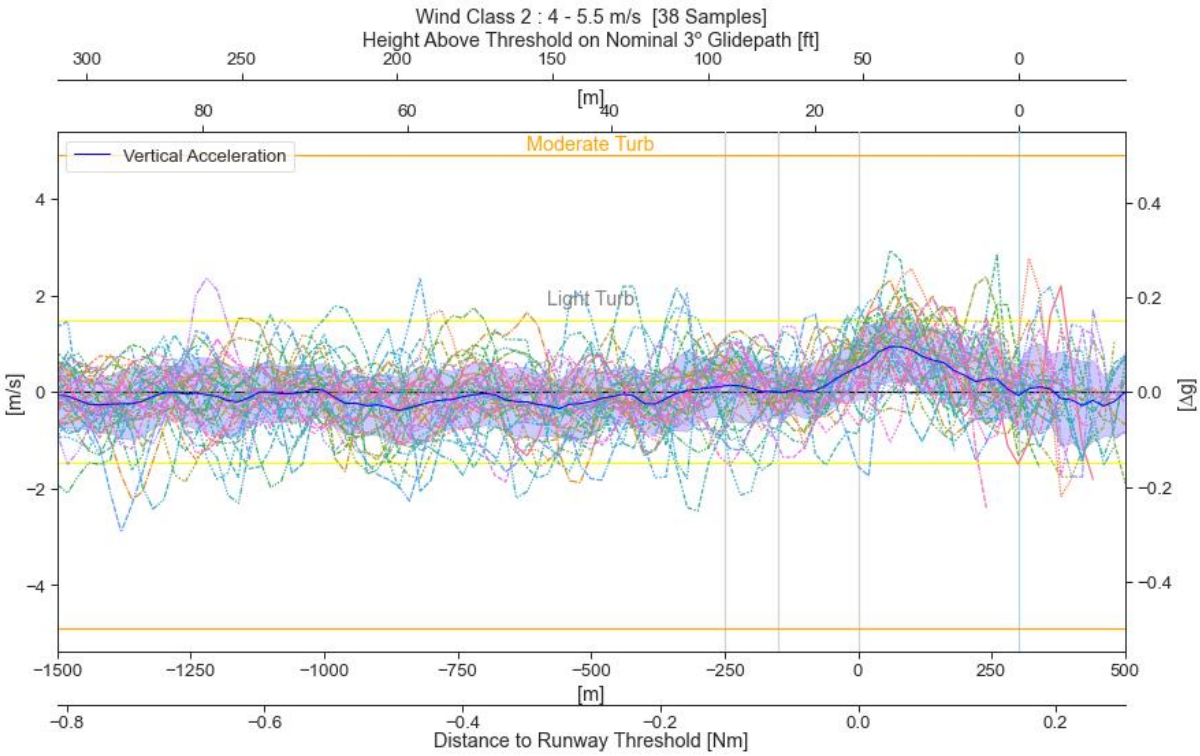
Wind Class 2 : 4 - 5.5 m/s [38 Samples]
Height Above Threshold on Nominal 3° Glidepath [ft]
300
250
200
150
100
50
0
[m]
80
60
40
20
0
Vertical Acceleration
Moderate Turb
Light Turb
4
2
0
−2
−4
[m/s]
0.4
0.2
0.0
−0.2
−0.4
[Δg]
−1500
−1250
−1000
−750
−500
−250
0
250
500
[m]
−0.8
−0.6
−0.4
−0.2
0.0
0.2
Distance to Runway Threshold [Nm]

(b)

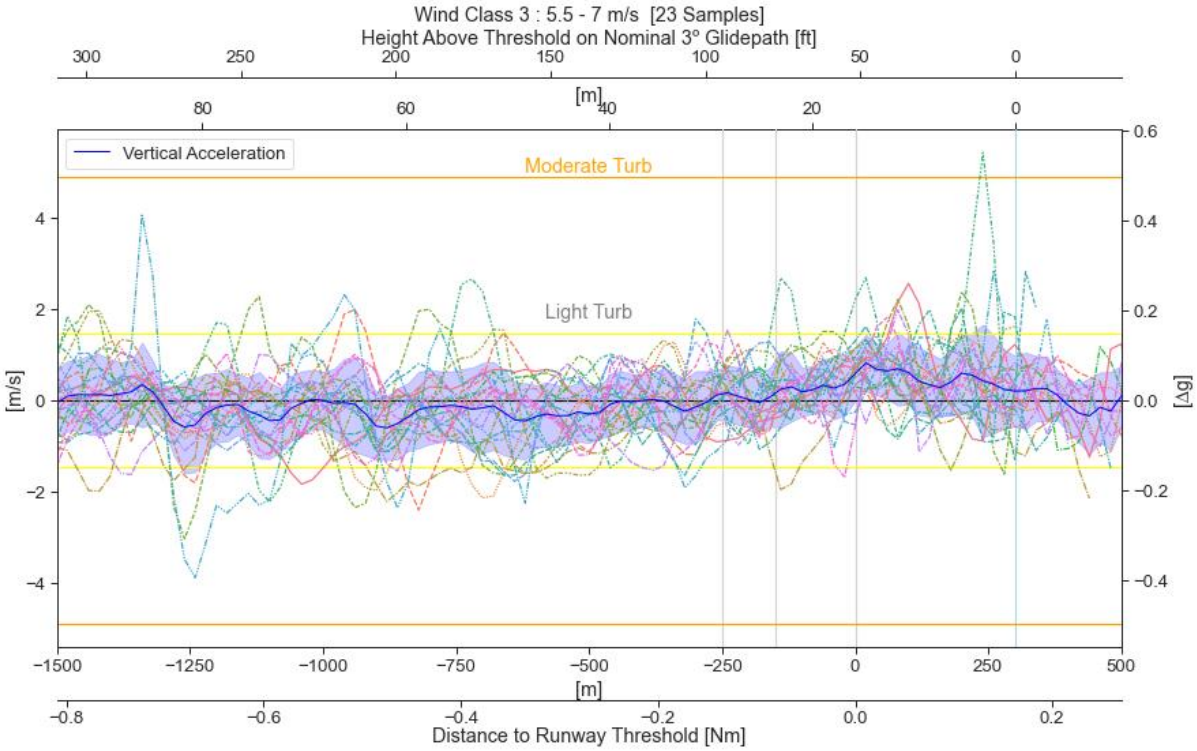

(c)

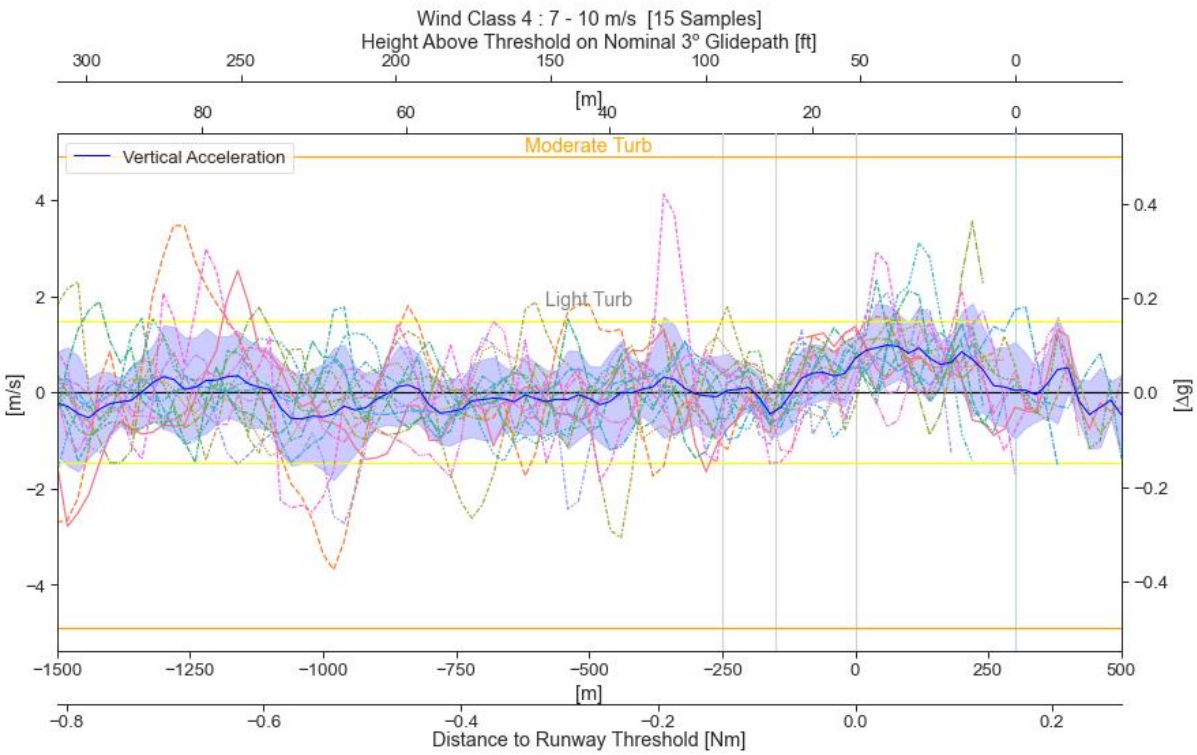

(d)

Figure 4.11 - Vertical Acceleration. The blue band around the mean represents one Standard Deviation.

4.3.2 Wind shear phenomena and hazard metrics

4.3.2.1 F-Factor

In aviation, windshear refers to a wind variation in intensity and/or direction over a given space or time-of-flight. This variation may be due to several meteorological phenomena, usually associated with convective weather or microbursts, but may as well be due to terrain influenced flows.

After several accidents due to windshear, a number of studies (mainly by NASA) [38] were conducted and measures adopted by the FAA [12] and later by other regulating bodies, to standardize and certify equipment capable of detecting and alerting of windshear presence. The principal parameter that emerged from these studies as operationally usable for crew alerting was the F-factor, which loosely translates the remaining capability (or lack thereof) of an aircraft to climb away from the ground in the presence of shear. It can be expressed as

$$F = \frac{\dot{U}_x}{g} - \frac{w}{V} \tag{35}$$

Where, $\dot{U}_x$ is the longitudinal wind variation with respect to time (Lagrangian derivative with reference on the aircraft), g is the acceleration of gravity, w the vertical wind component and V the True Air Speed. As may be deduced, the first term on the right represents the horizontal shear and the second term, the vertical shear.

It must be noted that a negative F corresponds to a performance increasing windshear, such as the reduction of tailwind or an updraft, and a positive F corresponds to a performance decreasing windshear.

This factor, when applied on a given instant may result in very large values for F, which are usually associated with atmospheric turbulence. These may be very short lived (as viewed from the flight progression perspective) and subsequently counteracted by large values of opposite sign, resulting in little effective performance deterioration. So, for a significant defect in performance to develop, a sufficiently large time must be considered in the application of the F-factor.

Lewis *et al* [39], when studying the adequate time for application on windshear alerting systems, argued that the take-off case and the approach case differ. While on the former the engines are already at high thrust upon encounter with a shear, on the latter the contrary happens.

Considering an initial reaction time of 5 seconds since performance starts to degrade until the pilot recognizes the hazard and acts upon it plus another 5 seconds for jet engine spool up to maximum power, there is a total of 10 seconds where performance is sub-optimal. See Figure 4.12 below

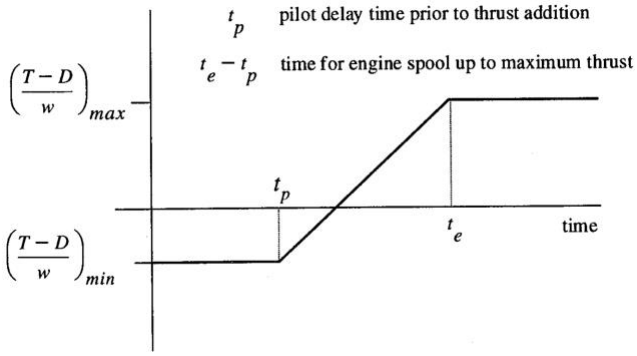

Figure 4.12 - Representative Energy profile for average F calculations. [39]

Assuming a standard approach glide path of 3°, a typical initial speed of 140 kts and allowing for a maximum speed loss of 25 kts and an altitude loss of 50 ft during a hazard encounter, the average F-factor over a distance (denoted as $\bar{F}$) can be calculated by

$$\bar{F}_{(s_0,L)} = \frac{1}{L}\int_{s_0}^{s_0+L} \frac{T-D}{W} ds - \frac{\Delta(V^2)}{2gL} - \frac{\Delta h}{L} \tag{36}$$

From this expression, considering $\frac{T-D}{W}$ progression as depicted on Figure 4.12 and for different distances L, the diagram of Figure 4.13 can be plotted.

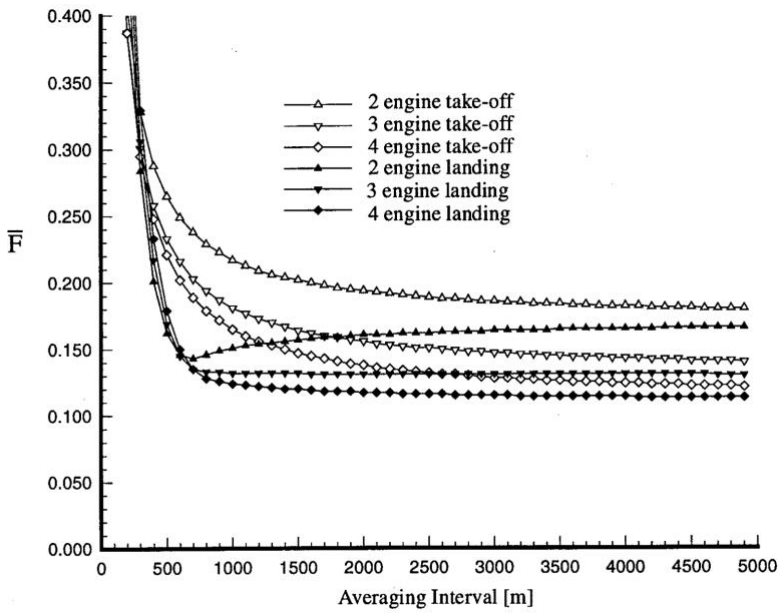

Figure 4.13 - Aircraft Performance Curves. [39]

From this it can be concluded that for a twin-engine on approach, the lowest $\bar{F}$ is 0.14 over a distance of 600m – which is roughly the distance covered in 10 seconds by an aircraft flying at 120kts. Bearing this in mind, the 161 flights present on this study were analyzed for an F-factor averaged over 10

seconds, as shown on Figure 4.14. On this figure, the plotted positions corresponds to the end of the 10 second window.

On these plottings is shown also a line corresponding to alert threshold of $\bar{F}$=0.105 mandated by the FAA on the Technical Standard Order TSO-C117(a) prescribing the minimum performance standards of airborne windshear warning systems for transport airplanes.[12]

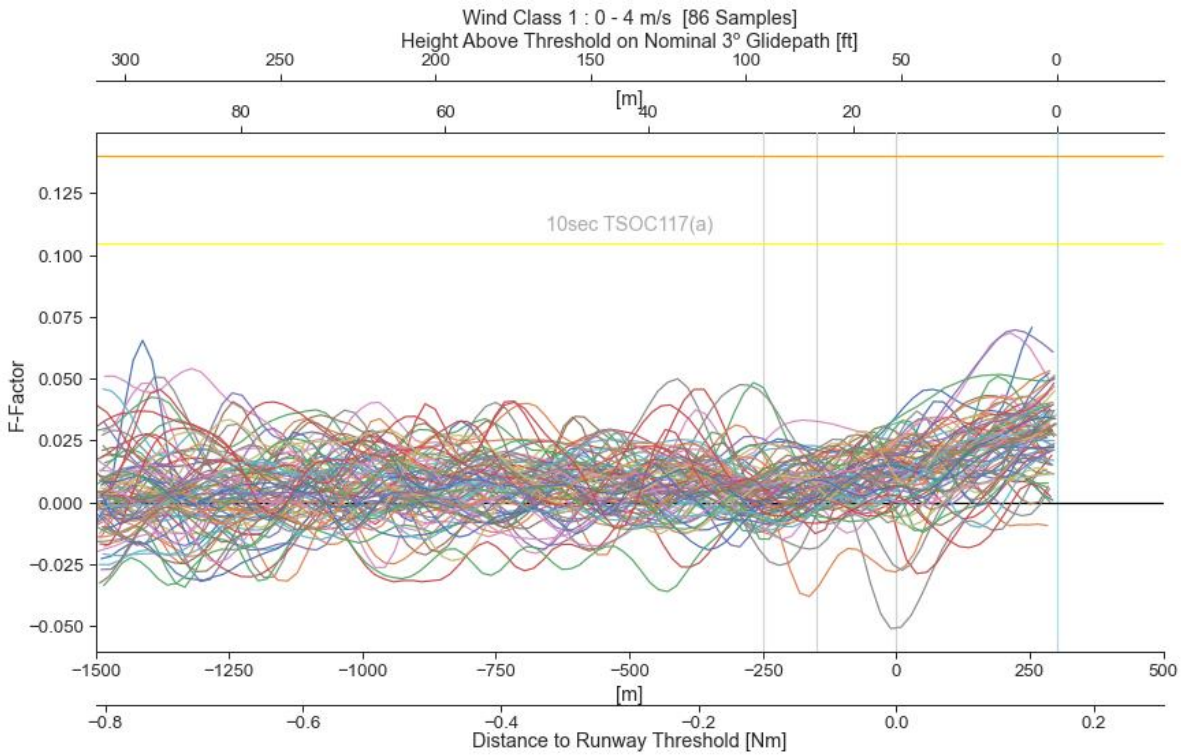

(a)

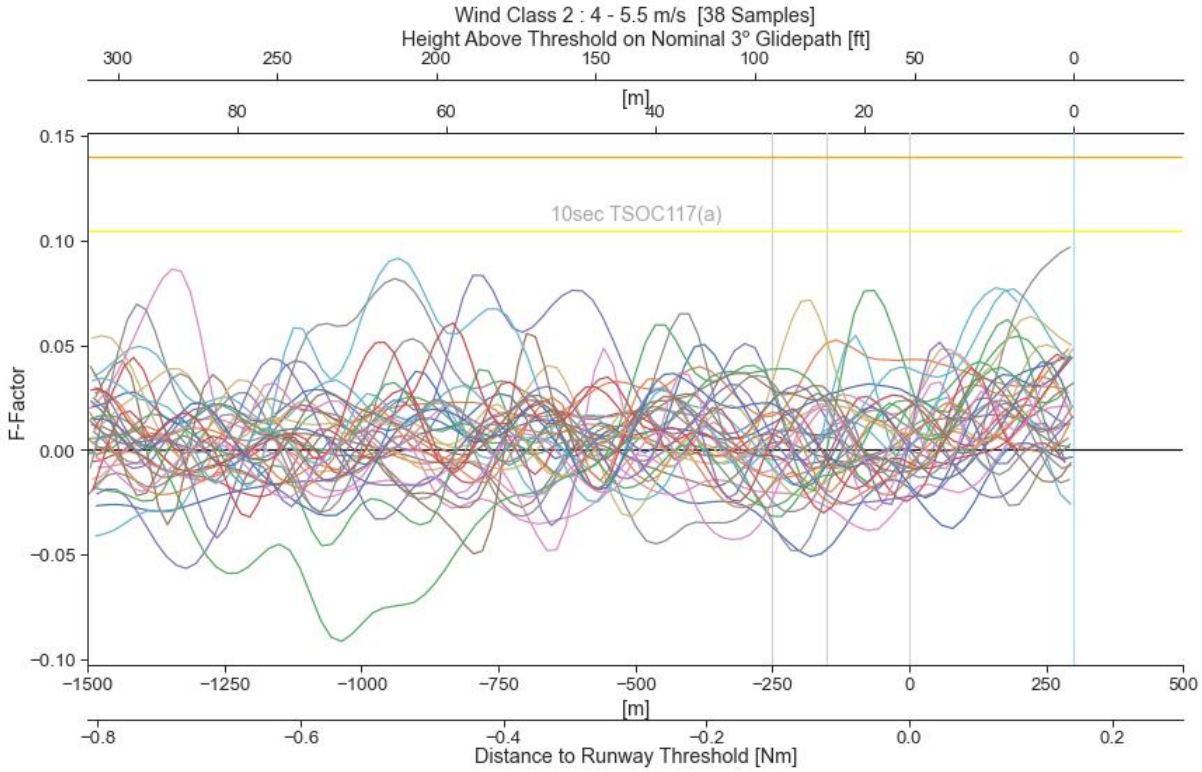
Wind Class 2 : 4 - 5.5 m/s [38 Samples]
Height Above Threshold on Nominal 3° Glidepath [ft]
300
250
200
150
100
50
0
[m]
80
60
40
20
0
0.15
0.10
0.05
0.00
−0.05
−0.10
10sec TSOC117(a)
F-Factor
−1500
−1250
−1000
−750
−500
−250
0
250
500
[m]
−0.8
−0.6
−0.4
−0.2
0.0
0.2
Distance to Runway Threshold [Nm]

(b)

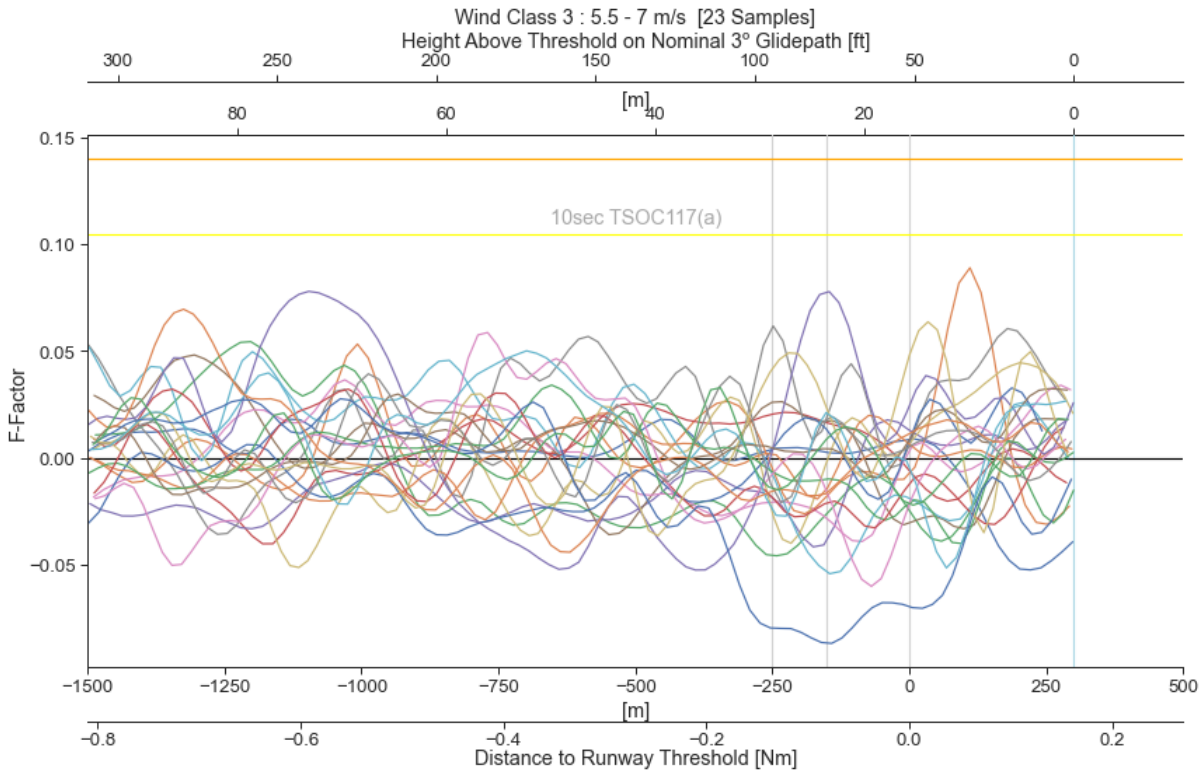
Wind Class 3 : 5.5 - 7 m/s [23 Samples]
Height Above Threshold on Nominal 3° Glidepath [ft]
300
250
200
150
100
50
0
[m]
80
60
40
20
0
0.15
0.10
0.05
0.00
−0.05
10sec TSOC117(a)
F-Factor
−1500
−1250
−1000
−750
−500
−250
0
250
500
[m]
−0.8
−0.6
−0.4
−0.2
0.0
0.2
Distance to Runway Threshold [Nm]

(c)

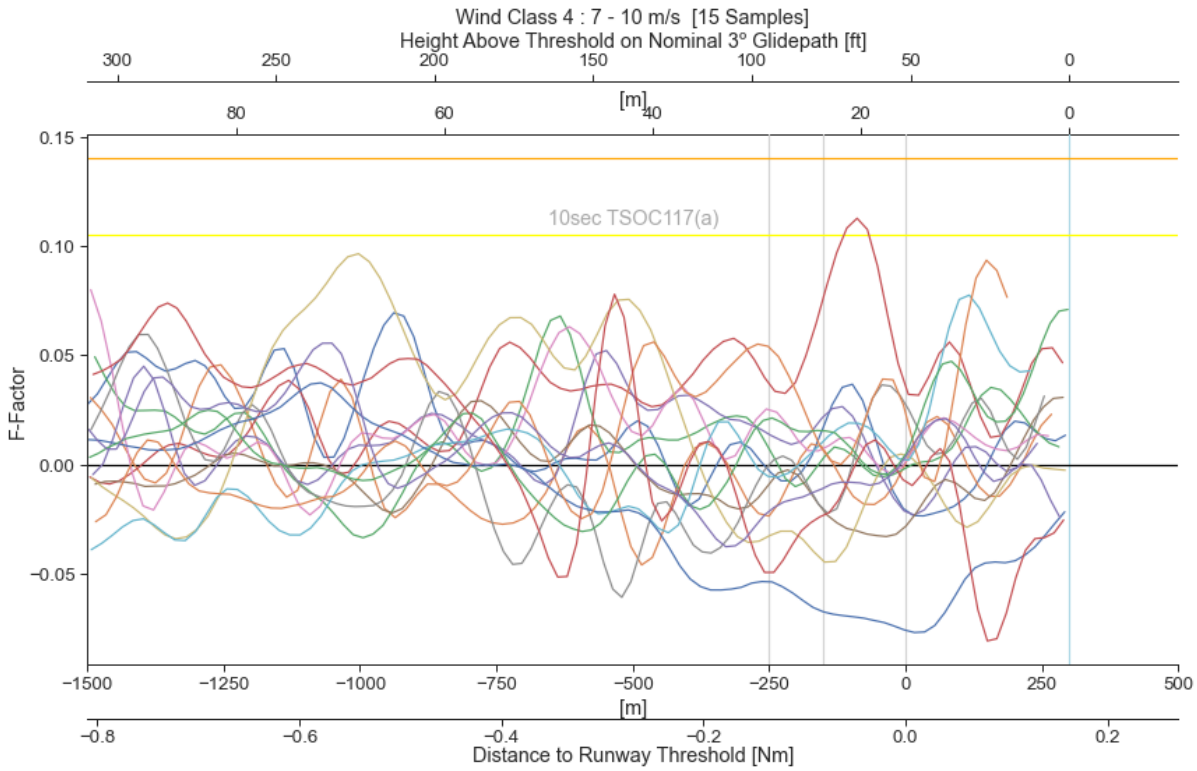

(d)

Figure 4.14 - F-factor average calculated over 10" for flights of each wind class. The Yellow line represents the FAA TSO-C117(a) criteria for alert.

On the analysis of these plottings it worth noting the relatively large $\bar{F}$ recorded for higher wind classes, particularly on the last 500 m to touchdown. Although the positive $\bar{F}$ are the performance degrading and hence the most dangerous, it must not be discounted the destabilizing effect of negative $\bar{F}$ at such late stage of the approach, possibly causing an overshoot of the landing aiming point and adding unnecessary and unwanted energy to the aircraft causing a long landing.

On the positive $\bar{F}$ cases (deteriorating performance), although not generally reaching the alert level, it must be considered that bellow a height of 200 ft any marked energy loss leaves the pilot little time for recovery and the risk of firm or uncontrolled ground contact is substantial. So, in this late stage of approach the alert level for $\bar{F}$ might be inappropriate.

4.3.3 Aircraft Dynamics and Stabilization Criteria

4.3.3.1 Bank Angle

During the studies to define a hazard criteria for aircraft encountering a wake vortex on final approach Simmonds *et al* [40] proposed the bank angle as means to define acceptable vs non acceptable aircraft conditions following a disturbance. Although this work was carried out on the said scope, it is appropriate to use the same metrics for turbulence induced roll as the situation does not differ significantly – both scenarios encompass an uncommanded aircraft movement at low altitudes.

On Figure 4.15, below, is proposed the maximum bank acceptable for a certain altitude, depending on aircraft type (size) and visibility conditions. The line of most similar condition to the case being studied on present work is the line representing the Boeing 707/720 on VFR.

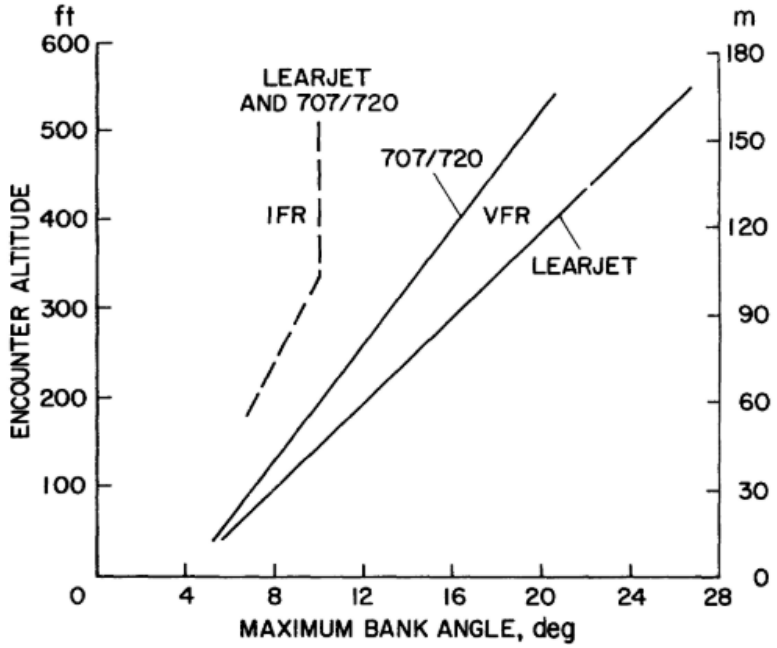

Figure 4.15 - Bank angle criteria as a function of proximity to the ground [40]

In order to compare and have a notion of the bank angles reached during the approach to runway 05, the bank histories were plotted for the last nautical mile until touchdown. See Figure 4.16 below.

It is important to note that it is not possible to determine if the bank was caused by turbulence action, pilot command or a blend of both. Either way, it is recognized that while most of the flights remain inside the hazard criteria, there are a few that go out. From the inspection of Figure 4.10 one can also observe that a significant number of flights have a late lineup with the runway and consequently induce a right bank exceedance; On the other hand, a left bank exceedance is very seldom the case. It can be observed on all wind classes that up until 1000m from the threshold there is a skew to the right.

Finally, it should be noted that for the higher wind classes, the bank angle dispersion is larger, visible also by the width of the Standard Deviation bands. This is expected due to the increased turbulence.

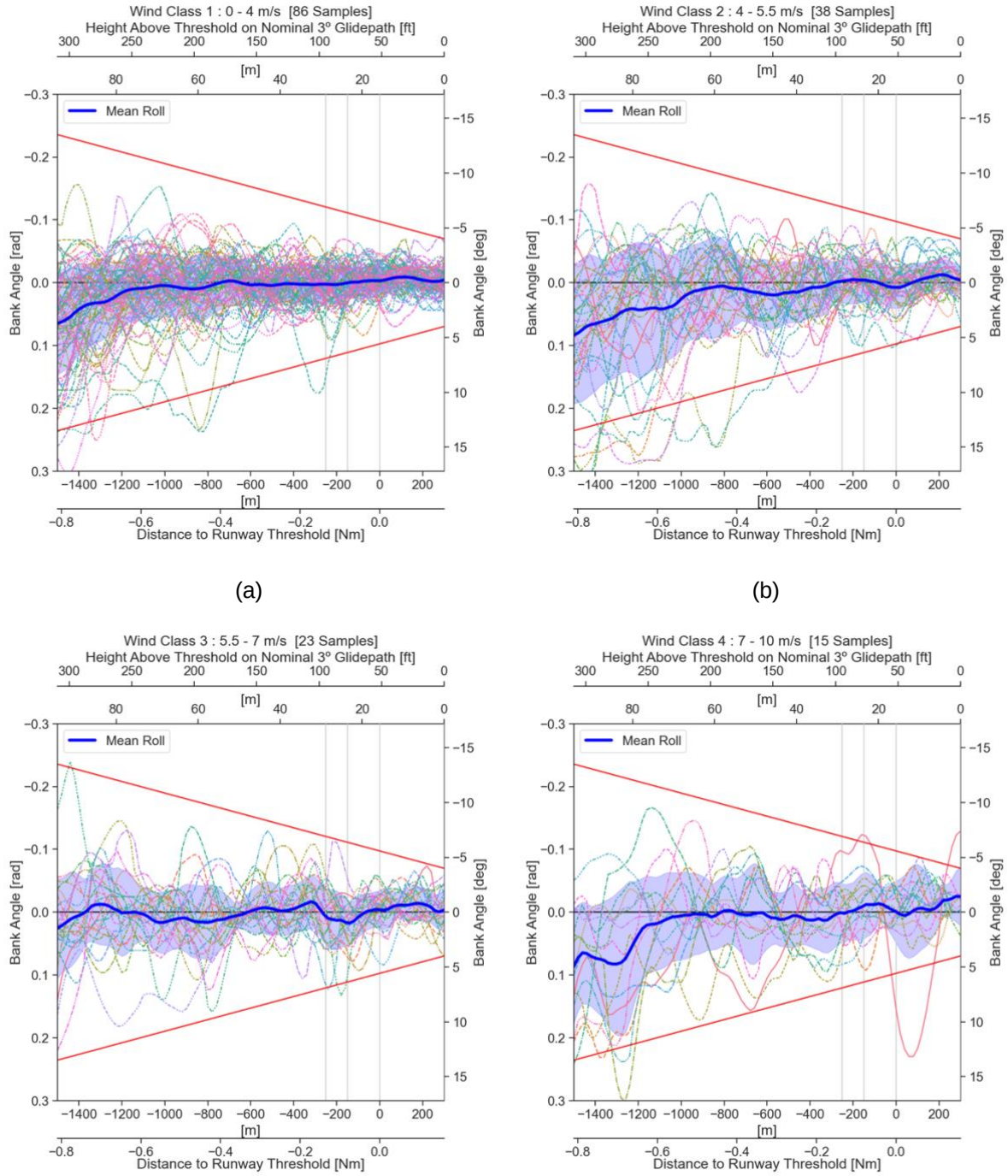

Figure 4.16 - Roll histories for the classes of wind considered. The red straight lines represent the roll hazard criteria proposed by Simmonds et al. The blue band represents one Standard Deviation. Positive angle is to the right.

4.3.3.2 Vertical speed on approach

As per the stabilization criteria mentioned on section 2.4.1, the vertical speed during approach should not exceed -1000 ft/min [≈-5 m/s]. It is worth noting that for this type of visual approach and while initially adjusting to intercept the PAPI glidepath it is natural that for a short period of time some exceedance is

observed. This can be noticed on the left side of the graphics of Figure 4.17. After being stabilized on the glide, it is not expected to see such exceedances except for very short spikes, due to turbulence perturbation and/or momentary adjustment.

It is generally noticeable that for higher classes of wind the amplitude and hence the dispersion of vertical speeds is higher.

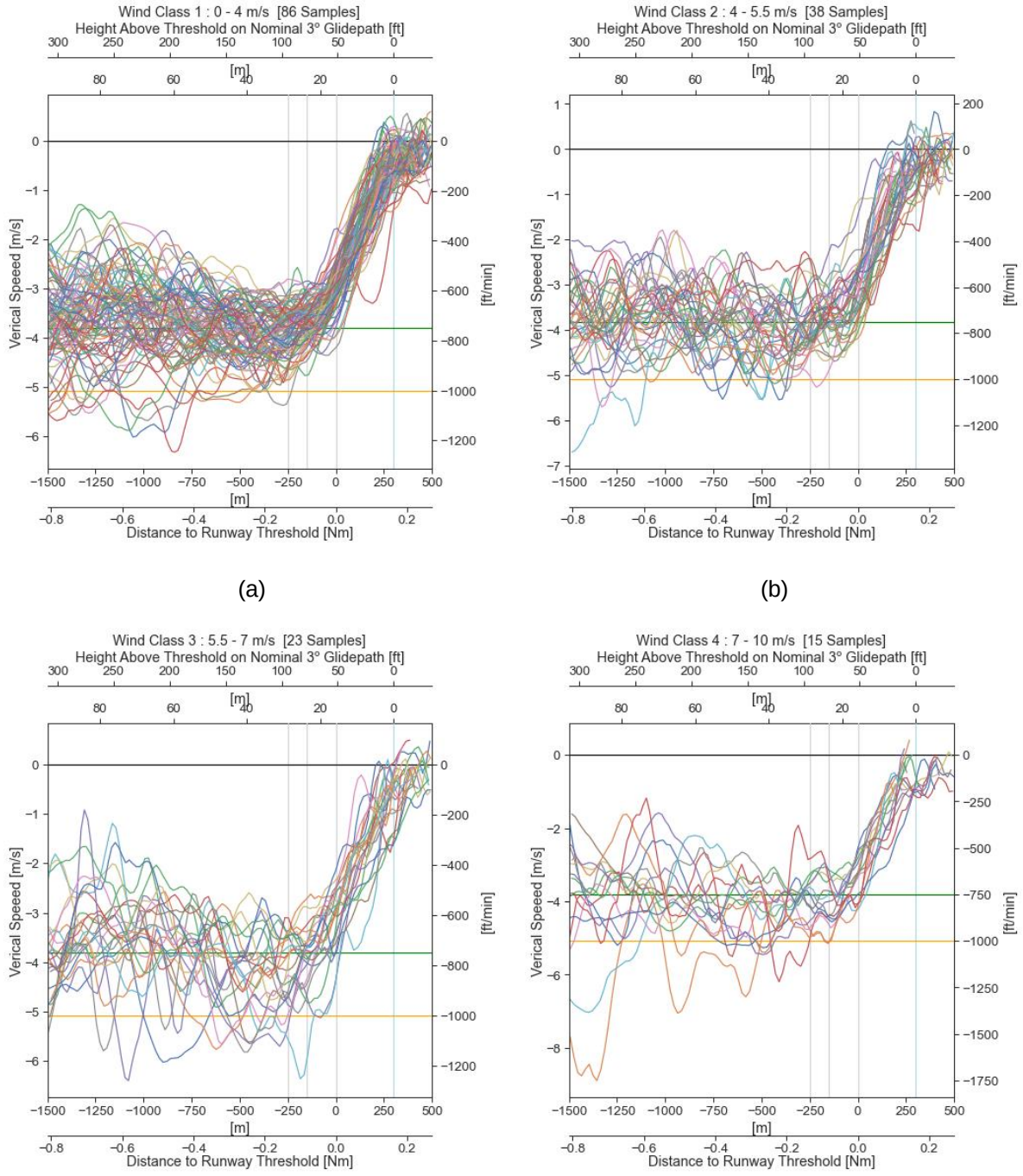

Figure 4.17 - Vertical speed during approach for the 4 classes of wind. The gren line represents the normal rate of descent and the orange line the 'alert' limit of 1000'/min.

4.3.3.3 *Speed Control*

The speed interval commonly accepted in the stabilization criteria is the target approach speed +10/-5 kts. It is clear to see on Figure 4.18 that for higher wind classes, the dispersion is greater but it is interesting to observe that occasionally there are exceedances on the fast side but there is none on the slow side. This is justifiable on strong and gusty conditions as pilots tend to prefer to fly faster to avoid the risk of stall due to a sudden lack of wind.

Also, some of the flights might have AutoThrust OFF, which may be a justification for some of the speed exceedances. During approach, when flying manually, pilots tend to privilege be in error by overspeed than the opposite, for the same reason as above.

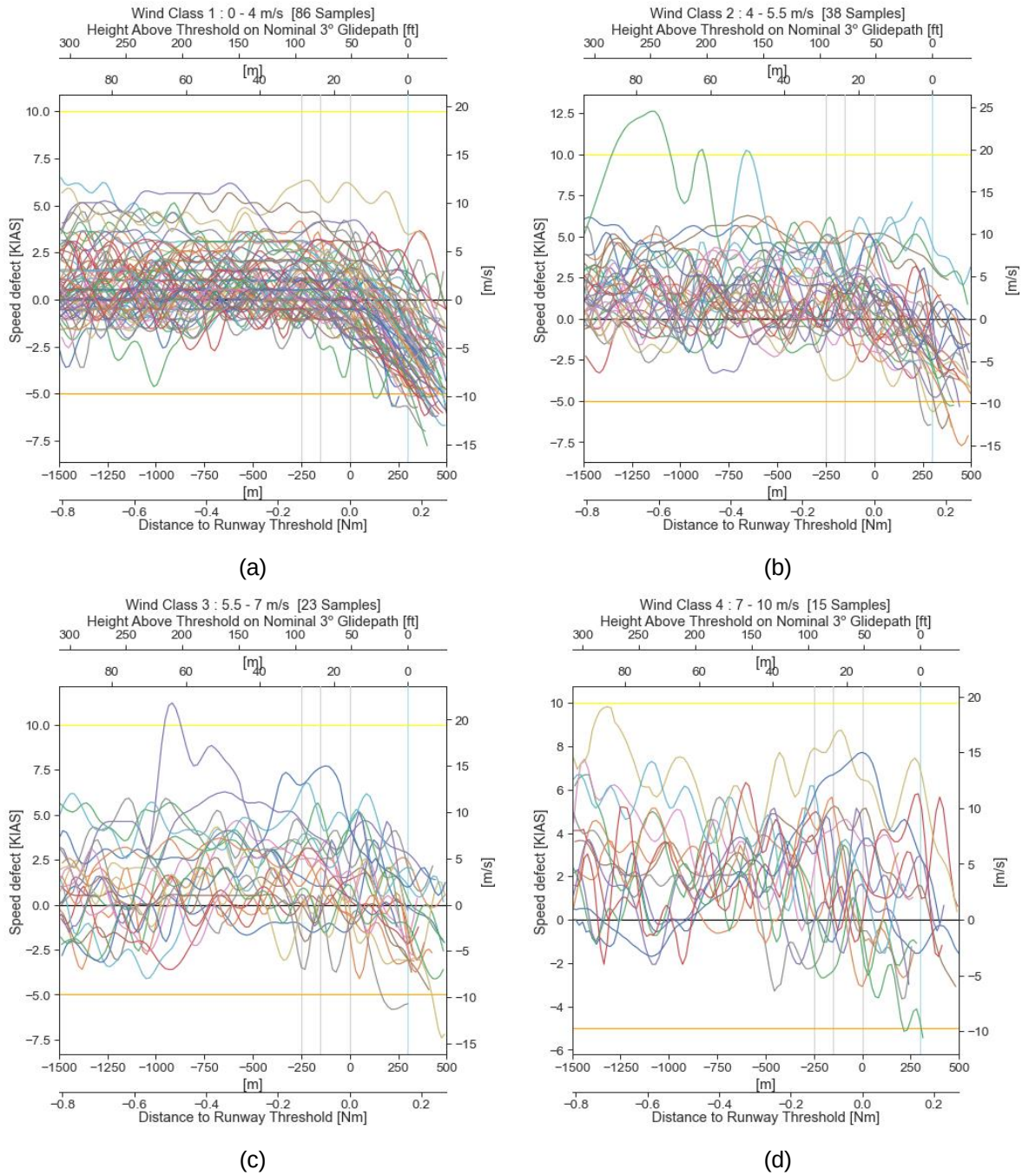

Figure 4.18 - Speed defect during approach.

4.3.3.4 *Vertical acceleration at touchdown*

The purpose of this analysis is to evaluate if the increasing surface wind intensity would correlate to heavier touchdowns, that is to say, with vertical speed not fully controlled.

A touchdown should not exceed a normal load factor of 1.8g and it can be seen from Figure 4.19 that there is no correlation of wind intensity (neither 2 minute mean nor instantaneous) with the normal load factor.

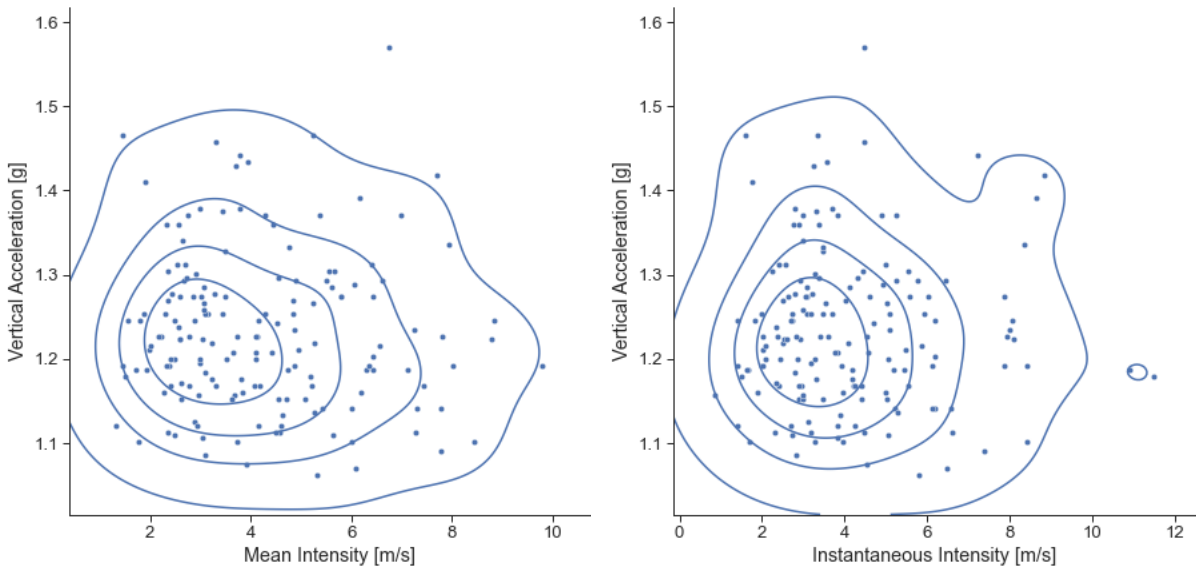

(a) (b)

Figure 4.19 - Vertical Load factor at touchdown. (a) considering 2' mean wind; (b) considering instantaneous wind.

5 Conclusions

On the end of this work, it is clear that the Madeira International Airport peculiar wind regimes and operational challenges continue to deserve a more profound study and just a small advance is made still through this present approach.

It is of notice the effort that must be spent on the initial treatment of data and the discrepancies that must be sorted before analysis or processing can be pursued. The data to be fused from multiple sources, sometimes has scant labelling or identification and must be harmonized as to the reference frames, corrected for bias and occasionally discarded altogether due to errors. So, it is of paramount importance that great attention is dedicated to the filtering, calibration and matching of data so that the fused dataset has the coherence necessary for posterior analysis. Not doing so will inevitably emerge further ahead as a greater hurdle.

On the assurance of compatibility of data, the use of the Rauch-Tung-Striebel filter smoother proved very robust in delivering coherent interpolation and adjustment to raw sensor measurement and was particularly useful on the flight path recreation.

Through the use of corrected angle of attack and estimated side slip, an estimation of the vertical local component of wind was made.

As for the wind regimes and their impact on the operation, it was not evident the existence of a strong correlation between the prevailing mean wind direction/intensity and a pattern of winds at specific points along the approach path. Rather, the stochastic nature of wind suggests that intermittent and possibly short-lived local phenomena take most of the responsibility for the sudden variation of airflow and consequent aircraft disturbance. Such conclusion is also suggested by the turbulence analysis.

The adaptation of the F-factor to present conditions showed that occasionally some flights suffer a late change of its energy level, but further investigation should be made to ascertain the validity of this metric at such late stage of approach.

The analysis of aircraft stabilization criteria showed generally that greater dispersion of parameters is to be expected in connection with greater wind intensities, but no clear pattern was detected in relation to other parameters.

5.1 What has been achieved

The major achievement of this work is the capability to extract all 3 components of the wind vector from the QAR data having due regard for the data preparation and coherence required to reach sound results.

The workflow and algorithm for this product, written in Python programming language, will be made available to flight data analysis personnel, for use on production work.

The use of the Rauch-Tung-Striebel filter smoother, although not at all new, also represents a positive step on the flight data handling.

Modest advance has been made on the understanding of the wind regimes at Madeira and their effects on landing aircraft, nevertheless the results reached may provide a basis for further understanding

5.2 Further work

During the execution of this work, a number of further advancements were felt to be of interest:

- For the same wind relative directions and intensities, compare the turbulence and its effects at Madeira with the effects felt at other airports on more benign conditions.
- Explore other wind directions, namely the sector from 300º to 040º, that is identified to be of operational concern.
- Use of machine learning algorithms on wind data and aircraft response to better identify patterns (if existent) and make better correlations of cause-effect.
- Decouple and filter out the pilot commands from the aircraft response to better extract the turbulence and wind shear induced maneuvering.
- Incorporate the control surfaces movement on the aerodynamic model, so as better valuate some key parameters such as C_L, C_D and body rotational moments.
- Investigate the adequacy or the adaptation of the concept of F-factor metrics for application bellow 200 ft altitude, during landing.

References

[1] Boeing Commercial Airplanes, “Statistical Summary of Commercial Jet Airplane Accidents,” *Boeing Commer. Airplanes*, p. 24, 2021, [Online]. Available: http://www.boeing.com/commercial/safety/investigate.html.

[2] International Civil Aviation Organization, “Doc 9817 Manual on Low-level Wind Shear,” 2005.

[3] NAV Portugal E.P.E., “AIP Portugal.” p. LP_AD_2_LPMA, 2021.

[4] Direção Regional de Estatística da Madeira, *Anuário Estatístico da Região Autónoma da Madeira 2019*. 2020.

[5] *Resolução da Assembleia Legislativa da Região Autónoma da Madeira n.o 26/2018/M*. 2018, pp. 4–5.

[6] EASA, “CS-25 Easy Access Rules for Large Aeroplanes,” 2021, [Online]. Available: https://www.easa.europa.eu/document-library/general-publications/easy-access-rules-large-aeroplanes-cs-25.

[7] ANAC, “Boletim Estatístico Trimestral Nº44, 4º trimestre 2019,” 2020.

[8] H. Haverdings and P. W. Chan, “Quick Access Recorder Data Analysis Software for Windshear and Turbulence Studies,” *J. Aircr.*, vol. 47, no. 4, pp. 1443–1447, Jul. 2010, doi: 10.2514/1.46954.

[9] L. Höhndorf, J. Siegel, J. Sembiring, P. Koppitz, and F. Holzapfel, “Reconstruction of aircraft states during landing based on quick access recorder data,” *J. Guid. Control. Dyn.*, vol. 40, no. 9, pp. 2387–2392, 2017, doi: 10.2514/1.G002637.

[10] J. Sembiring, L. Drees, and F. Holzapfel, “Extracting unmeasured parameters based on quick access recorder data using parameter-estimation method,” *AIAA Atmos. Flight Mech. Conf.*, pp. 1–12, 2013, doi: 10.2514/6.2013-4848.

[11] R. Huang, H. Sun, C. Wu, C. Wang, and B. Lu, “Estimating eddy dissipation rate with QAR flight big data,” *Appl. Sci.*, vol. 9, no. 23, pp. 1–14, 2019, doi: 10.3390/app9235192.

[12] FAA, “TSO-C117a, Airborne windshear warning and escape guidance systems for transport airplanes,” vol. 8, no. July 1988, pp. 1–80, 1996.

[13] R. L. Bowles, “Reducing Windshear Risk Through Airborne Systems Technology,” *ICAS*, pp. 1603–1630, 1990.

[14] L. B. Cornman, C. S. Morse, and G. Cunning, “Real-time estimation of atmospheric turbulence severity from in-situ aircraft measurements,” *J. Aircr.*, vol. 32, no. 1, pp. 171–177, 1995, doi: 10.2514/3.46697.

[15] WMO, “Aircraft Meteorological Data Relay (AMDAR) Reference Manual,” *World Meteorol. Organ. Doc. WMO-958*, 2003.

[16] H. Haverdings and P. W. Chan, “Quick Access Recorder (QAR) Data Analysis Software for Windshear and Turbulence Studies,” in *1st AIAA Atmospheric and Space Environments Conference*, Jun. 2009, no. June, doi: 10.2514/6.2009-3871.

[17] R. I. Sammonds and G. W. Stinnett Jr, “Hazard Criteria for Wake Vortex Encounters,” 1975.

[18] E. C. Hastings, G. T. Holbrook, and G. L. Keyser, “Preliminary Results of Simulated Vortex Encounters by a Twin-Engined Commercial Aircraft on Final Landing Approach,” 1980.

[19] E. Stewart, “A piloted simulation study of wake turbulence on final approach,” in *23rd Atmospheric Flight Mechanics Conference*, American Institute of Aeronautics and Astronautics, 1998.

[20] D. D. Vicroy *et al.*, “Characterizing the Hazard of a Wake Vortex Encounter,” *AIAA*, 1997.

[21] R. Luckner, G. Höhne, and M. Fuhrmann, “Hazard criteria for wake vortex encounters during approach,” *Aerosp. Sci. Technol.*, vol. 8, no. 8, pp. 673–687, 2004, doi: 10.1016/j.ast.2004.06.008.

[22] A. M. H. Nieuwpoort, J. H. M. Gooden, and J. L. de Prins, “Wind criteria due to obstacles at and around airports,” 2010. doi: NLR-TP-2010-312.

[23] M. Belo-pereira and J. A. Santos, “Air-Traffic Restrictions at the Madeira International Airport Due to Adverse Winds,” no. July 2007, 2020.

[24] “https://madeira.best/guia/factos-madeira/aeroporto-da-madeira-cristiano-ronaldo.” .

[25] “https://i.imgur.com/4z7FdJv.jpg.” .

[26] Flight Safety Foundation, “FSF ALAR Briefing Note 7.1 — Stabilized Approach,” *Flight Saf. Dig.*, no. November, pp. 75–80, 2000.

[27] J. Scavini, “Planche comparative de la famille des A320, en vue de côté.” 2011, [Online]. Available: https://commons.wikimedia.org/wiki/File:Airbus_A32X_family_v1.0.png%0A.

[28] J. Delhom, “Flight Data Analysis (FDA), a Predictive Tool for Safety Management System (SMS),” *Saf. First #17*, no. January, pp. 1–5, 2014.

[29] J. A. Gaspar, *Cartas e Pojeções Cartográficas*, 3rd ed. Lisboa: LIDEL, 2005.

[30] R. R. Labbe Jr, *Kalman and Bayesian Filters in Python*. 2018.

[31] S. S. Mulgund and R. F. Stengel, “Optimal nonlinear estimation for aircraft flight control in wind shear,” *Automatica*, vol. 32, no. 1, pp. 3–13, 1996.

[32] V. Klein and E. A. Morelli, *Aircraft System Identification: Theory and Practice*. 2006.

[33] J. G. Lowry and E. C. Polhamus, “A Method for Predicting Lift Increments Due To Flap Deflection At Low Angles of Attack in Incompressible Flow,” *Naca-Tn-3911*, p. 30, 1957, [Online]. Available: https://ntrs.nasa.gov/api/citations/19930084818/downloads/19930084818.pdf.

[34] G. W. Jones Jr., J. J. Concotta, and R. W. Walker, “Aerodynamic Forces on a Stationary and

Oscilating Circular Cylinder at High Reynolds Numbers," 1969. doi: NASA TR R-300.

[35] J. Wieringa, "Representativeness of wind observations at airports.," *Bull. Am. Meteorol. Soc.*, vol. 61, no. 9, pp. 962–971, 1980.

[36] ICAO, *Annex 3 to the Convention on International Civil Aviation Meteorological Service for International Air Navigation*, no. July 2007. 2007.

[37] S. H. Kim, H. Y. Chun, J. H. Kim, R. D. Sharman, and M. Strahan, "Retrieval of eddy dissipation rate from derived equivalent vertical gust included in Aircraft Meteorological Data Relay (AMDAR)," *Atmos. Meas. Tech.*, vol. 13, no. 3, pp. 1373–1385, 2020, doi: 10.5194/amt-13-1373-2020.

[38] D. D. Vicroy, R. L. Bowles, and R. H. Passman, "Airborne Wind Shear Detection and Warning Systems," 1992, doi: NASA CP-10105, Part 1.

[39] M. S. Lewis, P. A. Robinson, D. A. Hinton, and R. L. Bowles, "The Relationship of an Integral Wind Shear Hazard Aircraft Performance Limitations," 1994.

[40] R. I. Simmonds, G. W. Stinnett Jr., and W. E. Larsen, "Wake Vortex Encounter Hazard Criteria for Two Aircraft Classes," 1976. doi: NASA-TM-X-73113 and FAA-RD-75-206.

ANNEX 1 - Dataset Main Parameters

MAIN PARAMETERS ON DATASET				
Label	**Description**	**Samplg Freq [Hz]**	**Units**	**Interpolation / Smoothing**
TIME	Reference time	4	s	-
AC_TYPE	=	1	-	nearest
GWC	Gross Mass	1	ton	linear
CG	Center of Gravity Pos (in MAC)	1	%	linear
FQTYK	Fuel Quantity	1	kg	linear
LONFM_1	Position - Longitude	1	deg	RTS
LATFM_1	Position - Latitude	1	deg	RTS
BALT_1	Barometric Altitude	1	ft	RTS
RALT1	Radio Altitude	0,5	ft	cubic
ALT_CPT	Barometric Reference (QNH)	0,25	hpa	nearest
PITCH	=	4	deg	-
PITCH_RATE	=	4	deg/s	-
ROLL	Roll	4	deg	cubic
ROLR	Roll Rate	2	deg/s	cubic
YAW	Yaw rate	2	deg	cubic
TAS	True Airspeed	1	kt	cubic
VS_1	Stall speed	1	kt	linear
HEAD_MAG	Magnetic Heading	1	deg	circular cubic
HEAD_TRUE	True Heading	1	deg	circular cubic
TRACK_ANGLE_C	Magnetic Track	1	deg	circular cubic
DRIFT	=	1	deg	cubic
GSC	Ground Speed	1	kt	cubic
SATR	Static Air Temperature	1	ºC	linear
WIN_DIRR	Computed Wind Direction	1	deg	circular cubic
WIN_SPDR	Computed Wind Speed	1	kt	cubic
LONG	Longitudinal Acceleration	4	g	-
LATG	Lateral Acceleration	4	g	-
VRTG	Vertical Acceleration	4	g	RTS
AOAL	Angle of Attack Left	1	deg	cubic
AOAR	Angle of Attack Right	1	deg	cubic
PITCH_CPT	Commanded Pitch	2	deg	cubic
ROLL_CPT	Commanded Roll	2	deg	cubic
RUDPP	Commanded Rudder	2	deg	cubic
SPD_BRK_CMD	Commanded Speed Brake (Spoilers)	1	-	nearest
LDG_SELDW	Landing Gear selection	1	-	nearest
N11	Engine #1 N1	1	%	cubic
N12	Engine #2 N1	1	%	cubic
CONF	Slat/Flap Configuration	1	-	nearest
FPA	Flight Path Angle	1	deg	cubic
IVVR	Baro-Inertial Vertical Velocity	4	ft/min	RTS
LDG_STAT	Landing Gear Weight-on-wheels	1	-	nearest
ID_05	Instantaneous Wind Direction Rwy05	0,1	deg	circular cubic
II_05	Instantaneous Wind Intensity Rwy05	0,1	kt	cubic

ANNEX 2 - Kalman Filter and Rauch-Tung-Striebel Smoother Covariances Initialization

Diagonal Elements of Matrix [P]

Designation	State Variable	Variance
X Position Local Coords	x_L	4000 $(m)^2$
Y Position Local Coords	y_L	4000 $(m)^2$
Z Position Local Coords	z_L	2000 $(m)^2$
X Velocity Local Coords	$\dot{x}_L$	10 $(m/s)^2$
Y Velocity Local Coords	$\dot{y}_L$	10 $(m/s)^2$
Z Velocity Local Coords	$\dot{z}_L$	10 $(m/s)^2$
X Acceleration	$\ddot{x}_L$	0.1$(m/s^2)^2$
Y Acceleration	$\ddot{y}_L$	0.1$(m/s^2)^2$
Z Acceleration	$\ddot{z}_L$	0.1$(m/s^2)^2$
Heading	ψ	0.01 $(rad)^2$
Pitch	θ	0.01 $(rad)^2$
Roll	ϕ	0.01 $(rad)^2$

Matrix [Q] for horizontal x,y movement.

0.000730968	0.00584774	0.023391	0	0	0
0.00584774	0.0467819	0.187128	0	0	0
0.023391	0.187128	0.748511	0	0	0
0	0	0	0.000730968	0.00584774	0.023391
0	0	0	0.00584774	0.0467819	0.187128
0	0	0	0.023391	0.187128	0.748511

Matrix [R]

400	0	0	0	0	0	0	0	0	0
0	4	0	0	0	0	0	0	0	0
0	0	2.25	0	0	0	0	0	0	0
0	0	0	400	0	0	0	0	0	0
0	0	0	0	4	0	0	0	0	0
0	0	0	0	0	2.25	0	0	0	0
0	0	0	0	0	0	4	0	0	0
0	0	0	0	0	0	0	4	0	0
0	0	0	0	0	0	0	0	6400	0
0	0	0	0	0	0	0	0	0	6400